1 **T$_b$ or not T$_b$: Banding in Turbidite Sandstones**

2

3 Christopher J Stevenson[1*], Jeff Peakall[2], David M Hodgson[2], Daniel Bell[3], Aurelia Privat[2]

4 [1]School of Earth and Ocean Sciences, University of Liverpool,

5 [2]School of Earth and Environment, University of Leeds, LS2 9JT

6 [3]School of Earth and Environmental Sciences, University of Manchester, Manchester M13 9PL, U.K.

7 *Corresponding author: Christopher.Stevenson@liverpool.ac.uk

8

9 **ABSTRACT**

10 Recognition and interpretation of sedimentary structures is fundamental to understanding

11 sedimentary processes. Banded sandstones are an enigmatic sedimentary facies comprising

12 alternating mud-rich (as matrix and/or mud clasts) and cleaner sand layers. The juxtaposition of

13 hydrodynamically different grain sizes contradicts established models of cleaner sand bedform

14 development. Here, outcrop, subsurface core, and petrographic data from three deep-water

15 systems, with well-constrained paleogeographic contexts, are used to describe the range of

16 sedimentary textures, bedform morphologies and facies associations, and to quantify the mud

17 content of banding. Banding can occur in any part of a bed (base, middle or top), but typically

18 overlies a structureless basal sandstone or mud clast conglomerate lag, and is overlain by clean

19 parallel-laminated sandstone and/or ripple cross-lamination. Banding morphology ranges from sub-

20 parallel to bedforms that comprise low-angle laminae with discontinuous lenses of mudstone, or

21 asymmetric bedforms comprising steeply dipping foresets that transition downstream into low-

22 amplitude bedwaves, or steeply dipping ripple-like bedforms with heterolithic foresets. This style of

23 banding is interpreted as a range of bedforms that form progressively within the upper stage plane

24 bed flow regime via tractional reworking beneath mud-laden transitional plug flows. The balance of

25 cohesive and turbulent forces, and the rate of flow deceleration (aggradation rate), govern the style

26 of deposit. Banded sandstones and linked-debrites are rarely found juxtaposed together in the same

27 bed as they are distributed preferentially in proximal and distal settings, respectively. Understanding

28 the origins of banding in turbidite sandstones, the conditions under which it forms, and its

29 distribution across deep-water systems and relationship to linked-debrites, is important for it to be

30 used effectively as a tool to interpret the geological record.

31

32   **INTRODUCTION**

33

34 Banded sandstones have been described as alternating light (cleaner) and dark (mud-rich; as matrix

35 and/or mud clasts) parallel, sub-parallel or wavy layers within an otherwise clean turbidite

36 sandstone (e.g., Lowe and Guy, 2000; Lowe et al., 2003; Haughton et al., 2009; Hofstra et al., 2015,

37 2018). Our process understanding of banding is largely derived from analysis of deep-water deposits

38 in the Lower Cretaceous Britannia Formation and Paleogene Forties Fan in the North Sea

39 (Blackbourn and Thomson, 2000; Lowe and Guy, 2000; Lowe et al., 2003; Barker et al., 2008; Davis et

40 al., 2009; Haughton et al., 2009). Typically, banded sandstone divisions within the Britannia

41 Formation are thick (up to several meters) and occur overlying clean structureless basal sandstones

42 (Fig. 1; Guy, 1992; Blackbourn and Thomson, 2000; Lowe and Guy, 2000; Lowe et al., 2003; Barker et

43 al., 2008). Individual bands range in thickness from a few millimeters (microbanding), through 1-10

44 cm (mesobanding) and 10-50 cm (macrobanding), to >50 cm (megabanding) (Fig. 1). Banding

45 documented within the Paleogene Forties Fan is restricted to relatively thin divisions (up to 15 cm)

46 of microbanding that are sandwiched between a clean basal sandstone and an overlying linked

47 debrite; collectively forming hybrid event beds (Fig. 1; *sensu* Haughton et al., 2009). This style of

48   banding has also been reported from the Ross Formation, Ireland (Pierce et al., 2018) and the

49   Springar Formation., North Sea (Southern et al., 2017).

50

51   However, these data have important limitations. First, descriptions of banding are based on 10 cm

52   wide core, which inhibits recognition of larger wavelength bedforms. Therefore, it is entirely possible

53   that banding may comprise a more diverse range of bedforms, which would be identifiable in more

54   laterally extensive datasets. Second, there has been a limited amount of thin-section analysis of

55   banded sandstones published, which is restricted to averaged textural properties of both the light

56   and dark layers in the banded divisions (Lowe and Guy, 2000; Sylvester and Lowe, 2004). The

57   composition of individual bands is poorly quantified, which limits our ability to recognize banding in

58   the field, interpret its formational processes, and distinguish it from conventional sedimentary

59   structures, such as planar lamination (Bouma T_b division).

60

61   Banded sandstones have been documented within a variety of deep-water depositional

62   environments, occurring in either relatively proximal settings with clean sandstones (Kane and

63   Pontén, 2012; Hofstra et al., 2015, 2018; Spychala et al., 2017) or rarely in association with hybrid

64   beds in distal settings (Southern et al., 2017; Fonnesu et al., 2018), and specifically fan fringe settings

65   (Davis et al., 2009; Haughton et al., 2009; Pierce et al., 2018). Field observations of micro- to

66   mesobanding indicate that bands can be continuous, show thickness variations, or be discontinuous

67   over meters (Hofstra et al., 2015, 2018; Spychala et al., 2017; Fonnesu et al., 2018). Furthermore,

68   their morphology can be parallel, sub-parallel or wavy (Hofstra et al., 2015, 2018). Despite these

69   reports, there remains no systematic analysis of the morphology of banding, the paleogeographic

70   distribution of banding or its relationship to hybrid-bed deposition. This fundamentally limits our

71   ability to use banding as a facies to characterize and interpret deep-water depositional

72   environments.

73

74   The alternation of hydrodynamically different grain sizes within an individual deposit does not fit

75   with established models of bedform development. Such conventional models derived from clean

76   sand suspensions show that flow velocity and grain size are inter-dependent controls on bedform

77   development (e.g. Southard and Boguchwal, 1990; Southard, 1991; Van den Berg and van Gelder,

78   1993). In these cases, flow turbulence segregates particles enabling the flow to deposit discrete

79   grain size populations and diagnostic bedforms at different flow speeds (Baas et al., 2016). However,

80   banding indicates that hydrodynamically distinct sand and mud grain-size populations are deposited

81   under similar flow conditions in alternating layers. Two process models have been proposed to

82   explain the origin of banding; bedform development under mud-rich transitional flows (Baas et al.,

83   2011), and episodic near-bed turbulence damping (Lowe and Guy, 2000). The prominent model that

84   interprets banding as a product of cyclic near-bed damping of turbulence and modulating flow

85   behavior was derived from the subsurface Britannia Formation. In this model, periods of cleaner

86   sand deposition alternate with mud-rich bands formed as near-bed shear disintegrates mud flocs

87   and mud clasts resulting in increased cohesiveness and the development of a near-bed laminar plug

88   (Lowe and Guy, 2000). Haughton et al. (2009) emphasize longitudinal flow transformation; whereby

89   fine-grained cohesive particles are segregated towards the rear of the flow, which suppresses

90   turbulence and generates a cohesive laminar plug. In this case, banding is interpreted to be

91   generated beneath parts of the flow that are intermediate between turbulent and laminar

92   (cohesive), as the flow transforms along its length. These models place banding within a narrow

93   range of transitional flow conditions. However, recent experiments show that mixed sand/clay

94   suspensions can modify conventional bedform stability zones and produce a variety of heterolithic

95   deposits across a range of flow conditions (Baas et al., 2011, 2016; Schindler et al., 2015).

96   Outstanding questions in light of these advances include: Where does banding sit in relation to clean

97   sand bedforms, what textural and morphological properties distinguish banding from conventional

98   planar-laminated (T_b) sands, and what distribution does banding have in a turbidite facies tract?

99

100   We aim to document a range of banding textures and their facies associations from three ancient

101   deep-water systems. Our objectives are to: i) describe and quantify the varied sedimentological

102   character of banding, ii) place constraints on the spatial and stratigraphic distribution of banding,

103   and iii) discuss the formational processes responsible for banding. Addressing these objectives

104   permits us to present a model that links formational flow processes of banding with its stratigraphic

105   and spatial distribution in order to improve process understanding and prediction of deep-water

106   systems.

107

108   **Terminology**

109

110   **Flow types**

111   Herein, we use the term '*turbidity current*' to describe a flow that is non-cohesive and deposits

112   sediment incrementally, which deposits a '*turbidite*' (Bouma, 1962). We distinguish between low-

113   density flows that are dilute and turbulent, and high-density flows that have suppressed turbulence

114   and support grains via hindered settling effects (Lowe, 1982). '*Debris flows*' are cohesive with

115   sufficient clay content to suppress turbulence. They deposit *en masse* via frictional freezing to the

116   bed, which produces a '*debrite*' (e.g. Iverson, 1997; Talling et al., 2012). Flows are capable of

117   transformations between these turbulent and cohesive rheologies (Haughton et al., 2003; Felix and

118   Peakall, 2006). This can produce a hybrid deposit comprising a genetically-linked turbidite-debrite

119   within a single event bed, which is called a '*linked-debrite*' (Wood and Smith, 1958; Haughton et al.,

120   2003; Talling et al., 2012).

121

122   **Laminae**

123   Event beds contain divisions of sedimentary structures that are well-described in idealized facies

124   sequences (e.g. Bouma, 1962; Lowe, 1982; Haughton et al., 2009; Talling et al., 2012). These

125   divisions comprise structureless and laminated sandstones. '*Laminae*' are thin layers less than a

126   centimeter thick that occur in discrete divisions within an event bed. Laminae are grain supported

127   and have relatively sharp upper and lower boundaries, which denote a sharp change in grain size

128   and/or sorting (Campbell, 1967; Arnott and Hand, 1989; Best and Bridge, 1992). As laminae become

129   thicker (>5 mm) they tend to become more diffuse, whereby sorting values in the laminae are

130   progressively similar to that of the surrounding sandstone (Sumner et al., 2008).

131

132   **Mud and cohesivity**

133   'Mud' is typically defined in the field as a mixture of clay, silt, and organic fragments, with potentially

134   some very fine and fine sand (e.g. Winterwerp and van Kesteren, 2004; Kane et al., 2017). In terms

135   of the grain-size of the solid components mud is defined as clay plus silt (McCave et al., 1995;

136   Winterwerp and van Kesteren, 2004). The optical methodology used herein for the thin-section

137   analysis has a lower resolution limit for grains of ~60 μm, thus the material below the resolution

138   limit approximates to the <63 μm limit for 'mud'. Previous work on turbidites and linked-debrites

139   has shown that the analysis of mud in thin-section supports the qualitative observations of mud in

140   the field (Lowe and Guy, 2000; Kane et al., 2017; Bell et al., 2018a). A key question for the present

141   work however is whether this <63 μm fraction is composed of detrital clay minerals and thus is

142   indicative of deposition from cohesive flows. Whilst it is known that some silt-rich turbidites are

143   largely clay free (Strachan et al., 2016), we assume that the examples herein do contain detrital clay

144   based on the following. Turbidites and linked debrites from the Karoo, South Africa, the field area for

145   one of the examples herein, are known to contain between 10-35% clay, most of which is detrital in

146   origin (Kane et al., 2017). More generally, mud typically contains a significant proportion of clay,

147   particularly in deep-sea environments (Weaver, 1989; Winterwerp and van Kesteren, 2004;

148   Stevenson et al., 2014; Dutkiewicz et al., 2015). Lastly, even silt-dominated turbidites typically

149   contain appreciable (15-30%) clay (Piper, 1978; Stow and Piper, 1984) and exceptions are linked to a

150   range of grading styles and structures (Strachan et al., 2016), which are not observed in the

151   examples herein. We also recognise that inter-particle forces dictate that cohesive effects become

152   important (i.e. influence flow rheology and settling dynamics) at grain sizes <30 µm (McAnally et al.,

153   2007) whereby even quartz grains behave cohesively below 10 µm (McCave et al., 1995). Other

154   materials such as organic fragments and extracellular polymeric substances, that are ubiquitous in

155   deep-water environments, provide additional sources of cohesion in mud grain sizes (Craig et al.,

156   2020). Hence, we assume that our thin section measurements of mud contain appreciable clay, and

157   that the identification of mud in the sediments reflects cohesive forces in the flow from which they

158   were deposited.

159

160   **Definition of banding**

161   Here, we use the term '*Banding*' to describe alternating light and dark layers within a single event

162   bed. We distinguish between the alternating layers, and refer to dark, mud-rich layers as '*dirty*

163   *bands*' and lighter, cleaner sandstone layers as '*cleaner bands*'. Individual dirty bands are mud-rich

164   (as matrix and clasts), matrix supported, have very poor sorting, and are subdivided into mud-rich

165   dirty bands and sand-rich dirty bands based on their mud content. Individual cleaner bands are grain

166   supported, better sorted than dirty bands, and are subdivided into either mud-rich or sand-rich

167   cleaner bands based on their mud content. Thin section analysis presented in this study quantifies

168   the mudstone content across these different categories of band. Our definition in this paper differs

169   from previous work, where bands are recognized as couplets: a dark, mud-rich layer overlain by a

170   light, cleaner sandstone layer (e.g. Lowe and Guy, 2000; Haughton et al., 2009). In this study, we

171   demonstrate a variety of morphologies and contacts between dark, mud-rich layers and the lighter,

172   cleaner sandstone layers, which does not support the couplet model. Hence, we redefine the

173   definition of banding to accommodate these new insights.

174

175   **MATRIALS AND METHODS**

176   This study uses onshore borehole data and outcrops from the Karoo Basin, South Africa; offshore

177   subsurface core data from the Magnus Oilfield, North Sea, UK, and outcrops in several localities in

178   the Neuquén Basin, Argentina. Sedimentary successions in core and outcrop were logged at

179   centimeter-scale. Twenty-five thin sections were made from selected deposits in core and outcrop,

180   and were visually examined through a transmitted light optical microscope at 4× and 10×

181   magnification. Point counting was conducted using a petrographic microscope with 300 points per

182   slide to determine textural and compositional properties. Point counts were taken across several

183   areas on each slide, which were focused along individual bands (areas ~1-5 × 10 mm), and within the

184   cleaner sandstone divisions (areas ~5 × 10 mm). Grain-size was determined by measuring the

185   maximum diameter of optically distinguishable grains. Following Bell et al. (2018a), the limit of

186   optically resolvable grains was ~60 μm. Therefore, fine grains approximating to <63 μm are grouped

187   together and termed 'mud'. We first present each data set separately, as individual case studies,

188   then summarize commonalities across the data sets.

189

190   **Late Jurassic Magnus oilfield, North Sea**

191   **Geological Setting**

192 The Late Jurassic Magnus oilfield sits on the northeastern margin of the Viking Graben; perched to

193 the west of the Magnus-Penguin Basin in the North Sea (Fig. 2A). Accommodation developed in

194 response to a series of Permo-Triassic to Late Jurassic North Sea rifting episodes (Dominguez, 2007),

195 which influenced clastic depositional patterns across the oilfield (Fig. 2B) (Morris et al., 1999). The

196 Magnus Sandstone Member (herein MSM) is an approximately 120 m thick sand-rich turbidite

197 succession of Kimmeridgian age that is bounded above and below by the Kimmeridge Clay

198 Formation (Fig. 2C). From core facies and biostratigraphic data, the MSM stratigraphy is divided into

199 sub-units MSM-A through to MSM–G (Morris et al., 1999). An extensive core dataset from 27 wells

200 has permitted the spatial extent and character of MSM stratigraphy across the oilfield to be

201 constrained, which is interpreted in terms of three main depositional phases: (1) Late Kimmeridgian

202 with a depocenter in the mid-field, sourced from the northwest and displaying laterally confined,

203 fault-controlled channel-fill (MSM-A; Fig. 2B); (2) Early Volgian accretion of two depocenters forming

204 either side of the N-S trending Brent High (MSM-B, through to MSM-E to the SW; Fig. 2B); and (3)

205 Volgian as before but with the southward migration of the northern depocenter with fault

206 confinement (MSM-G) (Ravnås and Steel, 1997; Morris et al., 1999).

207

208 This paper uses core M16, from the central part of the field (Fig. 2B), which contains the full

209 stratigraphy described above. The interval examined here is MSM-C, a sand-rich turbidite succession

210 which overlies MSM-B, a mud-rich mass transport deposit (Haughton et al., 2009; Figs 2C and 3) .

211

212 **Results**

213 The MSM-C interval is a sand-rich turbidite succession, approximately 5 m thick but laterally

214 variable, which overlies an approximately 15 m thick mud-rich mass transport deposit (MSM-B). The

215 MSM-C turbidite succession is finer-grained and less well sorted compared with the rest of the MSM

216   turbidite stratigraphy with almost every bed recording some form of mud-rich division (Fig. 3).

217   Turbidites in this interval comprise thin- to medium-bedded (10-35 cm thick) fine-grained

218   sandstones with erosive and non-erosive basal surfaces and weakly graded bed tops, overlain by a

219   sharp grain-size break and a thin (2-5 cm) mud cap (Fig. 3). Banding occurs in a variety of positions in

220   the beds including: a) throughout a bed; b) from the base to middle parts of a bed, overlain by clean

221   planar-lamination and/or ripple cross-lamination; c) the middle parts of a bed, intercalated with

222   clean planar-lamination, and; d) towards the top of the bed, overlying a structureless sandstone

223   division.

224

225   Bands are parallel to sub-parallel, or can be low angle (5-9 degrees; measured relative to thin

226   bedded heterolithic intervals with flat concordant bases) with thicknesses ranging from millimeters

227   (Fig. 4A) up to 2 cm thick (Fig. 4B). Typically, dirty bands have sharp lower and upper contacts with

228   cleaner bands commonly loaded into their upper parts (Fig. 4C). Dirty bands have an elevated

229   proportion of mudstone as matrix and clasts (between 50-74%) compared to the surrounding

230   cleaner bands (between 25-39%). Dirty bands are typically matrix-supported, but vary in the amount

231   of sand they contain. Mud-rich dirty bands have isolated sand grains supported by the matrix (Fig.

232   4A, 4C). Sand-rich dirty bands have more sand grains, which tend to increase in abundance upwards

233   within the dirty band and pass from matrix- to grain-supported (Fig. 4B). Although the proportion of

234   sand grains may vary in the dirty bands, the maximum grain size is similar between dirty bands and

235   cleaner bands. Both mud-rich and sand-rich dirty bands also contain a large amount of rounded sub-

236   millimeter mudstone clasts, many of which are difficult to distinguish from the surrounding matrix

237   mudstone (Fig. 4).

238

239   Paleogeographic setting

240

241   Regional correlation of the MSM stratigraphy from the Magnus oilfield shows that it extends for 5-10

242   km southeast into the Penguin Half Graben (Ravnås and Steel, 1997). Within the Magnus oilfield, the

243   MSM succession is dominated by medium- to coarse-grained sandstones (Ravnås and Steel, 1997).

244   Hence, the MSM succession at Magnus is interpreted to represent a relatively proximal

245   paleoenvironment: a coarse-grained slope apron (Ravnås and Steel, 1997) or, drawing similarities

246   from recent outcrop work, an intraslope lobe complex (Spychala et al., 2015).

247

248   **Jurassic Los Molles Formation, Neuquén Basin, Argentina**

249   **Geological Setting**

250   The Neuquén Basin is located in central-western Argentina and central eastern Chile, and extends up

251   to 700 km in a north-south direction between latitude 32˚ S and 40˚ S (Fig. 5A). The basin is bounded

252   by wide cratonic areas of the Sierra Pintada System, the North Patagonian Massif, and the Andean

253   magmatic arc (Howell et al., 2005). During the Jurassic and Cretaceous, a post-rift back-arc basin

254   developed (Vergani et al., 1995; Franzese and Spalletti, 2001; Franzese et al., 2003; Howell et al.,

255   2005). The Lower-Middle Jurassic Cuyo Group represents the onset of marine deposition (Fig. 5B),

256   comprising pelagic and hemipelagic mudstone intercalated with successions of sandstone turbidites:

257   the Los Molles Formation (Gulisano and Gutiérrez Pleimling, 1995; Llambías et al., 2007; Paim et al.,

258   2008) (Fig. 5C). This paper examines exhumed turbidites from the Los Molles Formation in the west-

259   central sector of the Neuquén Basin at Location 1 about 15 km northeast of the town of Chos Malal,

260   and Location 2 in the southern sector at La Jardinera, to the southeast of the town of Aluminé (Fig.

261   5).

262

263   **Results**

264   **Chos Malal, Roadside Gully**

265   Outcrop of the Los Molles Formation (UTM 0360472/5872607) shows across depositional strike

266   exposures of banded sandstones over approximately 100 m with vertical exposures up to 2 m thick

267   (Fig. 6). The base of the package comprises a chaotic mudstone with abundant angular clasts of

268   mudstone and sandstone (Fig. 6A; below 1). This mudstone-rich facies is truncated by an erosion

269   surface (Fig. 6A; 1), which is variably overlain by a mudstone-clast conglomerate (Fig. 6A; between 1

270   and 2), and medium-bedded (20-30 cm thick) amalgamated banded sandstones (Fig. 6A; between 2

271   and 3). The succession is capped by a thick (1-2 meters) gravel conglomerate (Fig. 6A; above 3). Dirty

272   bands within the amalgamated sandstone are sub-parallel to wavy and discontinuous with sharp

273   bases and tops. They are either: i) thin (millimeters) primarily composed of small (mm diameter)

274   mudstone-clasts (Fig. 6B), or ii) thick (centimeters) bands composed of very small mudstone clasts

275   (sub-mm diameter) with an increased proportion of matrix mud compared to the surrounding

276   cleaner bands (Fig. 6C and 6D). Dirty bands have variable mudstone clast content with lateral grading

277   from mudstone clast conglomerate facies (Fig. 6A), to zones of banded sandstone composed of

278   abundant mudstone clasts, and banded zones with a relatively low proportion of mudstone (Fig. 6E).

279   These banded divisions with low mudstone content can have weakly developed lamination within

280   the cleaner bands (Fig. 6E). Typically, bands are sub-parallel to wavy and clustered into 3-10 cm thick

281   divisions showing pinch-and-swell morphologies over meters. They occur towards bed tops,

282   overlying structureless sandstone (Figs 6C and 6D).

283

284   **Chos Malal, Roadside Cutting**

285   Exposure of the Los Molles Formation (UTM 365568.08/5874549.43) at a similar stratigraphic

286   interval several kilometers down dip of the roadside gully outcrop shows amalgamated banded

287   sandstones (Fig. 7A). Here, beds comprise an erosional basal surface that is overlain by banded

288   sandstone. Where amalgamation is less pronounced, banded sandstones are overlain by a sharp

289   grain-size break and a relatively thin mudstone cap. The basal parts of beds can be marked by a

290   mudstone clast conglomerate lag or a structureless sandstone division. The banding is initially

291   cleaner and becomes more dirty upwards (Fig. 7B and 7C). Bands are sub-parallel in the lower parts

292   of the bed, which pass upwards into more complex heterolithic bedforms (Fig. 7B). Sub-parallel dirty

293   bands pinch and swell, and can be discontinuous over decimeters to meters (Fig. 7C facies B_{PS} and

294   B_{PM}). In contrast, the heterolithic bedforms are low-angle (5-7 degrees) with wavelengths between

295   15-30 cm (Fig. 7C facies B_{CL}). The low-angle bedforms grade upwards into shorter wavelength ripple-

296   like heterolithic bedforms with more consistently steeply dipping foresets (10 degrees) (Fig. 7C facies

297   B_{CR}).

298

299   **La Jardinera, Road Cutting**

300   The La Jardinera outcrop (UTM: 0349119/5638150) is exposed along a road cutting and shows the

301   strike architecture of a succession of thin- to medium-bedded (5-40 cm thick) medium-grained

302   sandstones (Fig. 8A). The succession is characterized by stacked structureless sandstone beds with

303   banded tops, or less-commonly banded bases. The basal structureless and banded sandstone

304   divisions are sharply overlain by a grain-size break and a thin mudstone cap (Figs 8B, 8C, 8D and 8E).

305   Thicker beds (30-40 cm thick) within the central part of the succession are bounded below by a

306   meter-thick interval of fine-grained thin beds, and above by another fine-grained thin-bedded

307   interval (poor exposure) and turbidites with linked-debrites (Fig. 8B). Linked-debrite bed divisions

308   found in the upper part of the succession contain weakly deformed elongate intraformational clasts

309   of banded sandstone, approximately 40 cm long and 10 cm thick (Fig. 8C). Sandstone beds are

310   generally ungraded but locally have coarser bases and normally graded tops. Banded divisions are

311   laterally variable in thickness (2-10 cm) over meters with sub-parallel bands pinching and swelling,

312 and commonly pinching out over meters (Figs 8D and 8E). Individual dirty bands have sharp upper

313 and lower contacts, are typically millimeters to centimeters thick, and are composed primarily of

314 mudstone clasts (Figs 9A). Mudstone clasts are sub-millimeter up to 1 cm in diameter, rounded and

315 elongate, poorly sorted with some clasts aligned with their long-axis sub-parallel to the dirty band

316 (Figs 9B and 9C). Individual dirty bands can have a uniform abundance of mudstone clasts

317 throughout (Fig. 9A), or show a progressive upward increase (Fig. 9B) or decrease (Fig. 9C) in the

318 amount of mudstone clasts through the dirty band. The overall proportion of mudstone (including

319 matrix and clasts) within the dirty bands is elevated (between 51-66%) compared to the surrounding

320 cleaner bands (between 32-40%).

321

322 Paleogeographic Setting

323 The Los Molles Formation comprises marine pelagic and hemipelagic mudstones, punctuated by

324 sandy turbidites (Gulisano and Gutiérrez Pleimling, 1995; Llambías et al., 2007; Paim et al., 2008).

325 The Chos Malal succession preserves banded sandstones with coarse beds of gravel and thick (1-2

326 meters) conglomerates (Figs 6A and 7A). The association of marine mudstones with very coarse

327 gravity flow deposits indicates this is a proximal setting: likely a lower slope or base of slope

328 environment. The La Jardinera succession preserves amalgamated packages of medium-grained,

329 thick-bedded sandstones that are separated by thinner-bedded heterolithic packages (Fig. 8B).

330 Towards the top of the logged section, linked debrites occur in association with a thin-bedded

331 heterolithic package. This is typical of compensational lobe stacking, whereby thick-bedded

332 amalgamated sandstones represent lobe axes and thinner-bedded sandstone with linked-debrites

333 representing lobe off-axis to lobe frontal fringe environments (Prélat et al., 2009; Spychala et al.,

334 2017). The coarse-grained nature of the sandstones coupled with compensational lobe stacking

335 suggests La Jardinera represents a relatively proximal lobe setting, either an intraslope or base of

336 slope environment.

337

Late Permian Skoorsteenberg Formation, Karoo Basin, South Africa

Geological Setting

The Karoo Basin is interpreted to have developed in the Permian through subsidence in response to subduction (Tankard et al., 2009) prior to developing as a retroarc foreland basin during the Early Mesozoic (Johnson, 1991; Cole, 1992; Visser, 1993). The Laingsburg depocenter in the southwest Karoo Basin consists of deep-water fill represented by the lower Ecca Group, specifically the Vischkuil, Laingsburg and Fort Brown formations (Fig. 10). These three formations comprise a 2 km thick shallowing-upward succession from distal basin-floor through continental slope to shelf-edge and deltaic settings (Fig. 10) (Wickens, 1994; Flint et al., 2011). This paper uses outcrop in the Laingsburg depocenter. The Laingsburg Formation is divided into Units A and B (Sixsmith et al., 2004; Brunt et al., 2013) (Fig. 10). Unit A is 350 m thick, comprising seven sandstone-prone sub-units (A1-A7), which are separated by regionally extensive mudstones. Here, we examine an outcrop in the Geelbeck River area within sub-unit A5 (Fig. 10).

351

Results

Laingsburg, Geelbek River, Unit A5

In general, sub-unit A5 in the Geelbek River is characterized by thick bedded fine-grained sandstones with low relief scours (Fig. 11A). Variable incision and amalgamation by overlying beds is common. Where amalgamation is less pronounced, sandstone divisions are sharply overlain by a grain-size break and a thin mudstone cap. Lenticular mudstone-clast lags typically overlie erosion surfaces (Sixsmith et al., 2004). Banding occurs in a variety of positions in beds with either erosive or non-erosive bases; most commonly towards the top of fine-grained structureless sandstone beds (Fig.

360   11A). However, it also occurs towards the base of beds overlain by parallel laminated sandstone, or

361   within the middle parts of beds, between basal structureless sandstone and overlying planar

362   laminated sandstone. Dirty bands comprise large amounts of small (millimeter diameter) rounded

363   mudstone clasts, and an increased proportion of mudstone within the matrix. Dirty bands are

364   millimeters to centimeters thick and have sharp upper and lower contacts with cleaner bands, which

365   are commonly loaded into the upper contact with the dirty band. Banding is present in a variety of

366   morphologies: sub-parallel and low-angle (4-9 degrees) bands that pinch-and-swell over meters

367   downstream (Fig. 11B), and more complex heterolithic bedforms (Fig. 11C). Figure 11C shows a

368   complex heterolithic bedform where the upstream (left side) of the bedform has relatively steeply

369   dipping (16 degrees), weakly climbing foresets with alternations of cleaner sandstone and dirty

370   bands. These foresets transition downstream (over decimeters to meters) into low-angle (5 degrees)

371   to sub-parallel banding (low-amplitude bedwaves). Thicknesses of cleaner and dirty bands vary

372   across the bedform.

373

374   Paleogeographic setting:

375   The Geelbeck area is interpreted to be situated on the proximal basin-floor (close to base-of-slope)

376   and close to distributive basin-floor channels within the axis of deposition of sub-unit A5 (Sixsmith et

377   al., 2004).

378

379   **Summary of characteristics of banding in turbidite sandstones**

380   Banding appears as 5-35 cm thick divisions of alternating light and dark bands within turbidite

381   sandstones. Bands typically occur within fine to very-fine grained sandstones (Figs 3, 6, 7 and 11) but

382   can also occur in coarser sandstone (Fig. 8). These banded divisions can occur in a variety of bed

383   positions, including towards the base, middle and upper parts (Figs 3, 6, 8 and 11), and can be

384 developed throughout a bed (Figs 3 and 7B). Banding can be found at the base, overlying an erosive

385 or non-erosive surface, whilst banding that occurs in the middle to upper parts of beds typically

386 overlies a basal structureless sandstone division (Figs 3, 6C, 8E, 11A) and/or a mudstone clast

387 conglomerate lag (Fig. 7A). Furthermore, banding can also be found intercalated with clean planar

388 laminated sands. Banding is commonly overlain by planar-laminated sandstone (Figs 4A and 7C), and

389 in some cases by ripple cross-lamination. Sandstone beds are typically amalgamated but where

390 amalgamation is less pronounced, banded sandstones are overlain by a grain-size break and a thin

391 mudstone cap. Dirty bands are intercalated with cleaner bands containing planar- and low-angle

392 laminae (Figs 4 and 7C, 11B). Banding forms a variety of morphologies and is laterally variable: sub-

393 parallel to low angle bands that pinch-and-swell over 1-3 meters (Figs 3, 7, 8, 11B) that may grade

394 laterally into mudstone clast conglomerate facies (Figs 6A and 6C); more complex heterolithic

395 bedforms with a mix of more steeply dipping foresets that transition downstream into decimeter-

396 wavelength low-angle bedwaves (Fig. 11C); or ripple-scale banded bedforms recording discontinuous

397 lenses of mudstone over 15-30 cm wavelengths (Fig. 7C; B_{CL} and B_{CR}). Individual beds can show an

398 upwards progression from sub-parallel banding into low-angle complex heterolithic banding, which

399 in turn transitions into shorter wavelength more steeply dipping heterolithic banding (Fig. 7C). In

400 terms of paleoenvironment, banding is generally found in proximal localities: base-of-slope channel

401 mouth settings of the Geelbek River, South Africa (Fig. 10) (Sixsmith et al., 2004; Hofstra et al., 2015),

402 and relatively proximal slope settings in the Magnus oilfield (Fig. 2) (Ravnås and Steel, 1997; Ravnås

403 et al., 2000), Chos Malal (Figs 6 and 7) and La Jardinera outcrops (Fig. 8). Commonly, banding occurs

404 in successions immediately overlying mud-rich substrates, where the beds have erosional basal

405 surfaces and contain an abundance of intraformational mudstone clasts (Figs 3 and 6A).

406 Bands generally have sharp upper and lower contacts with cleaner bands loading into dirty bands.

407 Dirty bands have an elevated proportion of mudstone as matrix and clasts (total mudstone content

408 typically 45-75%) compared to the cleaner bands (typically 25-45%; Figs 4 and 9), although there is a

409 continuum from sand-rich cleaner bands (~25-35%) through mud-rich cleaner bands (~35-45%) and

410   sand-rich dirty bands (~45-55%) to mud-rich dirty bands (~55-75%) (Fig. 12). Mudstone clasts within

411   individual dirty bands are sub-millimeter to 1 cm in diameter, rounded and elongate (Fig. 9). Their

412   abundance can be uniform, or decrease or increase upwards within an individual dirty band (Fig. 9).

413   The mudstone clasts are most likely a combination of recycled lithic mudstones (often several

414   millimeters in diameter and rounded) and softer muds eroded from the seafloor during the flow's

415   passage. These softer mud clasts exhibit a range of diameters but tend to be sub-millimeter,

416   irregularly shaped, and are often observed wrapped around grains or larger examples forming cm-

417   scale tendril-like shapes within the sandstones. The proportion of sand within a dirty band can vary

418   from a mud-rich dirty band with isolated floating sand grains to a sand-rich dirty band with a higher

419   proportion of sand (Fig. 12), and can increase in the amount of sand upwards and become grain-

420   supported at its top (Figs 4 and 6). Mud-rich dirty bands contain >55% mudstone, are matrix-

421   supported, and provide evidence for cohesive strength such as sheared fabrics and isolated floating

422   sand grains (e.g. Figs 4A and 4C). Sand-rich dirty bands are also matrix-supported but have a lower

423   mudstone content of ~45-55% and have an increased proportion of poorly sorted sand grains within

424   the bands (e.g. Figs 4B and 9A). They still retain features of poor grain segregation and shearing,

425   indicating deposition from a flow with cohesive strength (Iverson, 1997). Mud-rich cleaner bands

426   contain ~35-45% mudstone and are grain supported (e.g. Figs 4B and 6E). Finally, sand-rich cleaner

427   bands contain <35% mudstone, are grain supported and are better sorted than mud-rich cleaner

428   bands (Fig. 12). Sorting of grains is evidence of grain-by-grain deposition and traction beneath a

429   turbulent flow (Allen, 1982; Best and Bridge, 1992; Sumner et al., 2008). Identification of the

430   continuum of mud content from sand-rich cleaner bands to mud-rich dirty bands can be difficult to

431   distinguish visually, and thus banding is likely more prevalent than currently recognised.

432

433   **DISCUSSION**

434   **Origins of banding**

435   Banding comprises alternating mud-rich (dark) and cleaner sandstone (light) layers within a single

436   event bed. We recognize that the proportion of clay contained within the mud-rich layers is not

437   directly constrained by the point count measurements. However, as discussed earlier (see 'Mud and

438   cohesivity' section), we assume that the mud in the samples herein contains appreciable clay and

439   that elevated mud content reflects cohesive forces in the parent flows. Therefore, existing models

440   that interpret deposits as a product of cohesionless flows are not appropriate to interpret banded

441   sandstones, including: Low-Density Turbidites (Bouma, 1962), High-Density Turbidites (Lowe, 1982),

442   and Near-Bed Grain Flows (Mutti, 1992). Indeed, such models do not describe or attempt to

443   interpret heterolithic sedimentary structures. Currently, there are two competing process models

444   proposed to explain the origin of banding in sandstones; episodic near-bed turbulence damping

445   (Lowe and Guy, 2000), and bedform development under mud-rich transitional flows (Baas et al.,

446   2011, 2016).

447

448   *Episodic near-bed turbulence damping*

449   Lowe and Guy (2000) proposed that banding develops at the base of flows that vary between

450   turbulent and laminar states, through the cyclic development of near-bed cohesive plugs. These

451   plugs are postulated to form through episodic near-bed turbulence damping through electrical

452   charge induced bonding of clays, following disaggregation of clay flocs (Lowe and Guy, 2000). This

453   hypothesis was initially based on banded sandstones from the Lower Cretaceous Britannia

454   Formation, North Sea, which comprise sub-parallel mud-rich (matrix supported) bands that range in

455   thickness from a few millimeters (microbanding) through to >50 cm (megabanding) (Guy, 1992;

456   Blackbourn and Thomson, 2000; Lowe and Guy, 2000; Lowe et al., 2003; Barker et al., 2008; Fig. 1).

457   Banded sandstone divisions in this field can be up to several meters thick, and occur overlying clean

458   structureless sandstone. In the Britannia Formation examples, banding passes upwards into either a

459   clean planar-laminated sandstone, or more commonly into a mud-rich linked-debrite. Individual

460   bands are matrix-supported with clean sandstone loaded into their upper contacts and abundant

461   syn-sedimentary dewatering features, such as sheared and truncated pipes. The presence of thick

462   mega- and macro- bands with pervasive dewatering structures provides evidence for rapid

463   deposition. Later work on banding within hybrid beds has incorporated this process model and

464   linked it to longitudinal flow transformation, specifically a period between dominantly cohesionless

465   flow depositing high-density turbidites and more cohesive flow producing mud-rich sandstones and

466   debrites (Davis et al., 2009; Haughton et al., 2009; Southern et al., 2017). In this hybrid bed model, a

467   relatively thin (1-15 cm) banded sandstone occurs between a clean basal turbidite sandstone and an

468   overlying mud-rich linked-debrite within a single event bed. Individual bands are sub-parallel and

469   exhibit a sheared matrix- and loaded upper contacts. Bands may grade upwards from thicker,

470   muddier bands into thinner bands containing predominantly carbonaceous material (Davis et al.,

471   2009).

472

473   *Bedforms under mud-rich transitional flows*

474   In contrast to the concept of cyclical freezing of a near-bed plug, experimental work under

475   transitional flows (*sensu* Baas et al., 2009) with well-developed cohesive plugs has demonstrated

476   that banded deposits can form within the upper stage plane bed flow regime, and the washed out

477   ripple regime (transitional zone between true ripples and upper stage plane beds), via the migration

478   of bedforms over a period of >2 hours (Fig. 13) (Baas et al., 2011, 2016). Transitional plug flows form

479   through the presence of cohesive clay within a flow, which progressively modifies turbulence (from

480   enhanced to damped) as clay content increases. This results in the development of a laminar plug,

481   which grows downward from an interval of low shear stress (Baas et al., 2009). This transitional flow

482   behavior is governed by the balance of turbulent versus cohesive forces (Baas et al., 2009, 2011,

483   2016). Lower Transitional Plug Flows (*sensu* Baas et al., 2009) produced sub-parallel bands of muddy

484   sand overlain by low amplitude bedwaves comprising isolated streaks of clayey sand (Baas et al.,

485   2016). Over time, shallow scouring and the downstream migration of the bedwaves generated

486   complex asymmetric heterolithic stratification: steeply dipping lenses of cohesive clay foresets,

487   overlain by low-amplitude clayey sand bedwaves, which in turn were partially overlain by cleaner-

488   sand low-amplitude bedwaves. Upper Transitional Plug Flows (*sensu* Baas et al., 2009) produced sub-

489   parallel bands of sandy clay, which were overlain by heterolithic low-angle cross-laminated sand or

490   parallel-laminated cleaner sand (Baas et al., 2016). There have been indications from field

491   observations that banding can exhibit wavy morphologies (Hofstra et al., 2015, 2018). However,

492   there has been no field evidence for the presence of bedwaves, and low-angle and steeply dipping

493   foresets, which would support the experimental observations.

494

495   *Field evidence*

496   The examples of banding reported in this study are characterized by divisions 5-35 cm thick,

497   composed of individual bands that are millimeters to 2 cm thick. They occur in a variety of bed

498   positions and have a range of different morphologies including sub-parallel and low-angle, and

499   bedforms comprising both sub-parallel bands juxtaposed with low-angle and steeply dipping bands.

500   In addition, the mud content of individual dirty bands varies from matrix-supported mud-rich dirty

501   bands through to dirty bands with a higher proportion of sand grains (Fig. 12). Additionally, banding

502   reported in this study does not have strong syn-sedimentary dewatering features, such as sheared

503   pipe and dish structures. Rather, banding in this study shows more subtle loading structures (Fig.

504   4C). The morphologies and sedimentological characteristics of the banded sandstones documented

505   in our field data have similar characteristics to the thin and sharp heterolithic laminae produced in

506   the experiments of Baas et al. (2016) (Fig. 13). Examples of these similarities include the complex

507   asymmetrical heterolithic stratification in the Geelbek River (Fig. 11C); low-angle banding in the

508   Magnus core (Fig. 4A); and sub-parallel banding in La Jardinera (Fig. 8). Given the variety in

509   morphology, bed position and mud content observed in our examples, they are interpreted to be

510   the product of deposition (and reworking) from transitional flows with a sustained period of

511   traction, which have well-developed laminar plugs (Figs. 13 and 14; Baas et al., 2016). The clear

512   evidence for traction in many of these examples, through bedwaves and low- and steeply-dipping

513   foresets is incompatible with cyclic instantaneous freezing of a near bed plug flow, given that this

514   would allow no time for tractional movement. Hence, we interpret banding in these examples as the

515   product of tractional bedforms under sustained transitional flows (*sensu* Baas et al., 2009). Although

516   we did not observe strong dewatering structures (pipes and dishes) in the field examples, the

517   experiments of Baas et al. (2016) do report small-scale fluid-escape features in the more rapidly

518   aggraded deposits.

519

520   **Rate of flow deceleration**

521   In addition to the balance of cohesive versus turbulent forces, experiments with mixed sand/clay

522   suspensions show that the rate of flow deceleration fundamentally influences deposit character (Fig.

523   14). This is because deceleration is a primary control on aggradation rate, which governs the amount

524   of time the bed is exposed to traction (shear) from the overriding flow (e.g. Allen, 1982; Southard

525   and Boguchwal, 1990; Vrolijik and Southard, 1997; Leclair and Arnott, 2005; Sumner et al., 2008).

526   Rapidly decelerated cohesive suspensions (high clay content) produce debrite and linked-debrite

527   deposits without banding (Sumner et al., 2009; Baas et al., 2011). Cohesive flows that are

528   decelerated comparatively slowly generate sub-parallel banding (Baas et al., 2016). Less cohesive

529   flows (reduced clay content) at these longer deceleration times are able to produce more complex

530   banded sands (heterolithic bedforms of Baas et al., 2011, 2016). With even longer deceleration

531   times, near-bed turbulence (even in cohesive flows) has time to winnow the bed of fines, which

532   promotes segregation of clay/sand and results in largely clean laminated sand overlain by clay

533   (Malarkey et al., 2015; Baas et al., 2016) (Fig. 14).

534

Multiple depositional models for banding?

536 As interpreted here, banding can develop as bedforms beneath progressively aggrading transitional

537 flows (Baas et al., 2016). This mechanism is associated with relatively thin (millimeters to

538 centimeters) bands, which have a variety of bedform morphologies, and do not display strong syn-

539 sedimentary dewatering features (pipes and dishes); albeit experiments suggest some small-scale

540 dewatering features may be present (Baas et al., 2016). The exact character of the bands is governed

541 by the flow state: the balance of cohesive versus turbulent forces, and the rate of flow deceleration.

542 However, this tractional bedform mechanism may not be an explanation for the relatively thick (> 50

543 cm), matrix-supported, sub-parallel bands containing abundant syn-sedimentary dewatering

544 features, which characterize facies such as those in the Britannia Formation (Lowe and Guy, 2000)

545 and Springar Formation (Southern et al., 2017). Such sediments have largely been examined via core,

546 and there has not yet been evidence for cross-lamination (cross-stratification) and thus for traction

547 at the base of the flow. Furthermore, it seems unlikely that segregation of particles via traction

548 under a flow could generate such thick bands. Consequently, the postulated model for banding in

549 these systems, that they are produced via the cyclic deposition and rapid aggradation of near-bed

550 cohesive plugs (Lowe and Guy, 2000), remains the most plausible. Therefore, it appears that there

551 are two separate formative mechanisms for banding within deep-marine clastic sediments.

552

553 The transition between more fluidal flows and highly mud-rich debris flows, as is thought to occur in

554 hybrid beds (Haughton et al., 2009), will be dominated by transitional clay-rich flows (*sensu* Baas et

555 al., 2009). Considering the evidence presented herein that such flows are likely to produce banding

556 via tractional bedforms, given the correct transitional flow regime and deceleration profile, then it

557 would appear far more likely that such a mechanism is responsible for banding in hybrid beds, than

558   the Lowe and Guy (2000) model of cyclic freezing of near-bed plugs. This tractional-model for

559   banding in hybrid beds was first postulated by Baas et al. (2011), and the present work provides very

560   strong support for the importance of transitional flows (*sensu* Baas et al., 2009) in the formation of

561   hybrid bed banding.

562

563   ***T_b, or not T_b?***

564   Here, we have demonstrated that the field examples of banding are tractional bedforms and that

565   they are highly analogous to the transitional flow experiments of Baas et al. (2016) from the upper

566   stage plane bed (USPB) and washed out ripple (WOR) flow regime. Non-cohesive flows depositing in

567   the same regimes are associated with planar-lamination (Bouma T_b division) and low-amplitude

568   ripples (Bouma T_b/T_c division boundary), respectively. Banding in the examples herein occupies a

569   similar position within a vertical facies succession as clean parallel-lamination. It occurs: i) towards

570   the top of beds overlying structureless sandstone, ii) as a basal division overlain by parallel-

571   laminated sandstone and/or ripples, iii) in the middle parts of beds sandwiched between basal

572   structureless sandstone and overlying parallel-laminated sandstone, or iv) is intercalated with clean

573   planar-laminated sandstone. As banding occupies similar flow regimes as parallel-lamination (i.e.

574   USPB and WOR) and occurs at a similar positions within vertical facies successions as T_b parallel-

575   laminated sandstones, it suggests that banding represents the T_b division for clay-rich transitional

576   flows, with moderate rates of deceleration (see section on Rate of flow deceleration). Given this

577   conclusion, we suggest that the Bouma T_b clean sandstone division and banding may occupy a

578   similar position along a turbidite facies tract. However, the spatial relationship between banded

579   bedforms and true T_b lamination is made complicated by the nature of flow transformation from

580   turbulent to cohesive transitional flow states; this evolution can in turn be related to a facies tract.

581   We explore this concept below.

582

Distribution of Banded Sandstones and Linked-Debrites

584   Here, we use examples of banded sandstones and linked-debrites from the literature alongside

585   insights gained from this study to propose a conceptual distribution of these facies across deep-

586   water systems (Fig. 15). This study recognizes banding within intraslope basins (Figs 2 and 3; Fig. 15A

587   Part i), base-of-slope channel mouth settings (Fig. 10; Fig. 15A Part ii), and less well-constrained

588   proximal slope settings (Figs 6 and 7). Previous work has also associated banding with proximal

589   settings (Barker et al., 2008; Kane and Pontén, 2012; Southern et al., 2017), and specific deep water

590   environments including: channel splays (Fig. 15A Part iii) and immediately overlying mud-rich MTD's

591   (Davis et al., 2009); immediately down-dip of channel-mouth scours (Hofstra et al., 2015), and at

592   base-of-slope lobes (Fig. 15A Part ii) (Spychala et al., 2017; Hofstra et al., 2018). In contrast, banded

593   sandstones in distal settings are rarely reported. Instead, linked-debrites without an intermediary

594   banded division are common (Fig. 15A Part iv), comprising clean basal sandstone directly overlain by

595   mud-rich chaotic sandstone (Talling et al., 2004, 2007; Amy and Talling, 2006; Davis et al., 2009;

596   Haughton et al., 2009; Lee et al., 2013; Talling, 2013; Fonnesu et al., 2015, 2018; Spychala et al.,

597   2017; Mueller et al., 2017). Where banded sandstones occur in distal fan fringe settings, they are

598   relatively thin divisions (up to 15 cm) sandwiched between the clean basal sandstone and the

599   overlying mud-rich linked-debrite (Haughton et al., 2009). Confining slopes may also influence the

600   distribution of banded sandstones and linked-debrites (Fig. 15A Part v). Examples of both banded

601   sandstones and linked-debrites have been associated individually with mud-draped confining

602   topography (Barker et al., 2008; Patacci et al., 2014; Southern et al., 2017; Bell et al., 2018b). Indeed,

603   if confinement is pervasive along the length of a deep-water system then banded sandstones may be

604   expected in more distal settings, such as documented in the Springar Formation, North Sea

605   (Southern et al., 2017).

606

607   **A model for banding in submarine fans**

608   Given that banding and hybrid beds are both linked to cohesive, clay-rich flows, why is it that

609   banded sandstones are rarely part of the same hybrid bed and are associated with different deep

610   water environments? We propose that the rate of deceleration in transitional flows, along with the

611   balance of cohesive versus turbulent forces, controls the distribution of banded sandstones and

612   linked-debrites (Figs 14, 15B and 15C). In relatively proximal locations, flows are likely to be quasi-

613   steady with a sustained period of velocity and low rates of deceleration, whilst in more distal

614   settings flows are more likely to be unsteady and subject to rapid deceleration via catastrophic

615   collapse of flow turbulence (Fig. 15B) (Kane et al., 2009, 2017; Stevenson et al., 2014). Proximal

616   quasi-steady transitional flows will produce periods of sustained traction, which promotes the

617   development of a variety of banded bedforms (Fig. 15C). Their exact morphology will depend on the

618   cohesive strength of the flow, the near-bed turbulence, and the amount of time the bed is reworked

619   (Fig. 14). Rapid flow deceleration in distal settings results in rapid aggradation and the suppression

620   of traction. Without sustained traction, banded bedforms are not able to develop. Instead, when

621   cohesive forces dominate over flow turbulence, a thick cohesive plug develops, which deposits *en*

622   *masse* as a debrite (Fig. 15C). This idealized distribution can be perturbed. Flows that entrain large

623   volumes of mud and/or exceptionally cohesive mud in proximal localities can transform rapidly into

624   cohesive flows, which locally deposit linked-debrites within 100's of meters down dip of the site of

625   erosion (Fig. 15C) (Fonnesu et al., 2015, 2018; Southern et al., 2015; Brooks et al., 2018). Confining

626   slopes may force local changes in rates of flow deceleration, resulting in the deposition of either

627   linked-debrites (Patacci et al., 2014; Bell et al., 2018b) or banded sandstones (Southern et al., 2017).

628

629   **Recognition criteria for banding**

630   Banding in the field or in core is recognized as alternating dark (dirty) and lighter (cleaner) layers

631   occurring within a single event bed. Bands have an elevated proportion of mud compared to the

632   surrounding cleaner sandstone divisions ranging from grain-supported sand-rich cleaner bands (>25-

633   45% mud content) through to matrix supported mud-rich dirty bands (45-75% mud content). These

634   are similar to average mud contents reported from banded sandstones in the Britannia field (18-

635   30%), with dirty bands potentially having twice the amount of mud compared to the cleaner bands

636   (Lowe and Guy, 2000). Key differences between banding and T_b parallel-laminated sandstones are: i)

637   an elevated proportion of mud (25-75%; this study) compared to clean planar-laminated sandstone

638   (5-10%; Sylvester and Lowe, 2004; Stevenson et al., 2014); ii) the dirty bands are matrix supported in

639   contrast to grain-supported layers in T_b; iii) cleaner and dirty bands both exhibit poor sorting within

640   bands, unlike T_b which is well sorted within individual laminae; iv) banding comprises alternating

641   layers with each band demarcated by a sharp change in mud content whilst T_b exhibits abrupt

642   changes in sorting between laminae (Allen, 1982; Best and Bridge 1992; Sumner et al., 2008); v) dirty

643   bands may have a sheared matrix and commonly exhibit small-scale dewatering features, such as

644   loading of cleaner bands into dirty bands, whereas deformation is absent in T_b, and, vi) the

645   morphology of bands includes low-amplitude bedwaves punctuated by steeply dipping heterolithic

646   foresets, and shorter wavelength higher-amplitude ripple-like heterolithic structures, in addition to

647   sub-parallel layers similar in shape to T_b parallel-lamination. Despite these criteria, the range of

648   lower mud contents in banded sandstones can in some cases make it difficult to distinguish banding

649   visually from clean T_b parallel-laminated sandstone in outcrop and core, and thus banding is likely to

650   be under recognized.

651   Recognition criteria for differentiating between banding formed by traction under transitional flows

652   as described herein, as against those formed by episodic near-bed turbulence damping (Lowe and

653   Guy, 2000) are: i) the close relationship between banding and Bouma T_b in vertical facies successions

654   for transitional flows; ii) spatial variations in morphology (e.g., discontinuous down-dip; low-angled

655   bedforms; bedwaves; steeply dipping foresets) present in transitional flows whilst turbulence-

656 damped banding is always sub-parallel; iii) macrobanding (10-50 cm thick) and megabanding (>50

657 cm thick) are solely associated with episodic turbulence damping, as these are too thick to form

658 under traction; and, iv) pervasive syn-sedimentary dewatering structures such as sheared and

659 truncated pipes are associated with turbulence damping, reflecting far more rapid deposition than

660 under tractional regimes. Whilst, the morphological criterion is only applicable in outcrop, the other

661 criteria can be utilized in both field and core.

662

663   **CONCLUSIONS**

664 We examine banding within turbidite sandstones using a suite of outcrop and core data from three

665 different deep-water systems: the Lower Jurassic, Magnus Oilfield, North Sea; the Lower Jurassic

666 Neuquén Basin, Argentina, and the Permian Karoo Basin, South Africa. Bands are recorded in very

667 fine- to medium-grained sandstones in a variety of bed positions including base, middle and top.

668 Banding occurs above, erosive and non-erosive basal surfaces, mudstone lags, or structureless sands,

669 and is overlain by clean parallel-laminated sandstones and/or ripple cross-lamination. Banded

670 divisions may also be intercalated with planar lamination. Individual dirty bands are relatively thin

671 (mm to cm) and have an elevated proportion of mudstone (between 45-75% as matrix and clasts)

672 compared to intercalated cleaner bands (between 25-45%), although a continuum of mud content is

673 recognized from sand-rich through to mud-rich cleaner bands, and sand-rich to mud-rich dirty

674 bands. Banded divisions range in thickness (5-30 cm), mud content and morphology (from sub-

675 parallel to composite heterolithic bedforms). Banded sandstones occur in proximal settings that are

676 situated close to sites of erosion into muddy substrates. This style of banding is interpreted to

677 comprise a range of bedforms that form progressively within, and at the boundaries of, the upper

678 stage plane bed regime via tractional reworking beneath mud-laden transitional plug flows. The

679 conditions under which banding can develop are similar to those of planar-laminated (T_b) sandstone,

680 the primary difference being an elevated proportion of cohesive mud within the flow. The balance of

681   cohesive versus turbulent forces, and the rate of flow deceleration (aggradation rate) govern the

682   style of deposit. Banded sandstones and linked-debrites rarely overlie each other within the same

683   bed, and are associated with proximal and distal deep-water environments respectively. The rate of

684   flow deceleration is key to explaining this distribution, whereby in proximal settings, slow rates of

685   deceleration subject the bed to a period of traction (producing banding), whilst in distal settings

686   flows rapidly decelerate resulting in minimal traction (producing debrites). This model of banding in

687   the T_b flow regime is in marked contrast to earlier work invoking cyclic aggradation of near-bed

688   cohesive plugs, although such plugs provide an explanation for much thicker bands that lack

689   evidence of traction, suggesting that banding can be polygenetic. Understanding the origins of

690   banding and the conditions under which it is formed, its distribution across deep-water systems, and

691   its relationship to linked-debrites, is important for it to be used effectively as a tool to interpret the

692   geological record.

693

694   **Acknowledgements**

705

706   **References**

707

708   Allen, J.R.L., 1982. Sedimentary structures: their character and physical basis, Volume 1. Amsterdam,

709   Elsevier.

710   Amy, L.A., Talling, P.J., 2006. Anatomy of turbidites and linked debrites based on long distance (120 x

711   30 km) bed correlation, Marnoso Arenacea Formation, Northern Apennines, Italy.

712   Sedimentology, v. 53, p. 161–212. doi:10.1111/j.1365-3091.2005.00756.x

713   Arnott, R.W.C., Hand, B.M., 1989. Bedforms, primary structures and grain fabric in the presence of

714   suspended sediment rain. Journal of Sedimentary Petrology, v. 59, p. 1062–1069.

715   Baas, J.H., Best, J.L., Peakall, J., 2016. Predicting bedforms and primary current stratification in

716   cohesive mixtures of mud and sand. Journal of the Geological Society of London, v. 173, p. 12–

717   45. doi:10.1144/jgs2015-024.

718   Baas, J.H., Best, J.L., Peakall, J., 2011. Depositional processes, bedform development and hybrid bed

719   formation in rapidly decelerated cohesive (mud-sand) sediment flows. Sedimentology, v. 58, p.

720   1953–1987. doi:10.1111/j.1365-3091.2011.01247.x

721   Baas, J.H., Best, J.L., Peakall, J., Wang, M., 2009. A phase diagram for turbulent, transitional, and

722   laminar clay suspension flows. Journal of Sedimentary Research, v. 79, p. 162–183.

723   doi:10.2110/jsr.2009.025.

724   Barker, S.P., Haughton, P.D.W., McCaffrey, W.D., Archer, S.G., Hakes, B., 2008. Development of

725   rheological heterogeneity in clay-rich high-density turbidity currents: Aptian Britannia

726   Sandstone Member, UK continental shelf. Journal of Sedimentary Research, v. 78, p. 45–68.

727   doi:10.2110/jsr.2008.014.

728 Bell, D., Kane, I.A., Pontén, A.S.M., Flint, S.S., Hodgson, D.M., Barrett, B.J., 2018a. Spatial variability in

729   depositional reservoir quality of deep-water channel-fill and lobe deposits. Marine and

730   Petroleum Geology, v. 98, p. 97–115. https://doi.org/10.1016/j.marpetgeo.2018.07.023

731 Bell, D., Stevenson, C.J., Kane, I.A., Hodgson, D.M., Poyatos-Moré, M., 2018b. Topographic controls

732   on the development of contemporaneous but contrasting basin-floor depositional

733   architectures. Journal of Sedimentary Research, v. 88, p. 1166–1189. doi:10.2110/jsr.2018.58.

734 Best, J., Bridge, J., 1992. The morphology and dynamics of low amplitude bedwaves upon upper

735   stage plane beds and the preservation of planar laminae. Sedimentology, v. 39, p. 737–752.

736 Blackbourn, G.A., Thomson, M.E., 2000. Britannia Field, UK North Sea: petrographic constraints on

737   Lower Cretaceous provenance, facies and the origin of slurry-flow deposits. Petroleum

738   Geoscience, v. 6, p. 329–343. doi:10.1144/petgeo.6.4.329.

739 Bouma, A.H., 1962. Sedimentology of some Flysch Deposits: A Graphic Approach to Facies

740   Interpretation. Elsevier, Amsterdam/New York, 168 pp.

741 Brooks, H.L., Hodgson, D.M., Brunt, R.L., Peakall, J., Hofstra, M., Flint, S.S., 2018. Deep-water

742   channel-lobe transition zone dynamics: Processes and depositional architecture, an example

743   from the Karoo Basin, South Africa. Geological Society of America Bulliten, v. 130, p. 1723–

744   1746. doi:10.1130/B31714.1.

745 Brunt, R.L., Hodgson, D.M., Flint, S.S., Pringle, J.K., Di Celma, C., Prelat, A., Grecula, M., 2013.

746   Confined to unconfined: Anatomy of a base of slope succession, Karoo Basin, South Africa.

747   Marine and Petroleum Geology, v. 41, p. 206–221. doi:10.1016/j.marpetgeo.2012.02.007.

748 Campbell, C.V., 1967. Lamina, laminaset, bed and bedset. Sedimentology, v. 8, p. 7–26.

749   doi:10.1111/j.1365-3091.1967.tb01301.x

750 Cole, D., 1992. Evolution and development of the Karoo Basin. *in* Witt, M.J. Ransome, I.G.D., eds.,

751   Inversion Tectonics of Capre Fold Belt, Karoo and Cretaceous Basins of South Africa: Balkema,

752   Amsterdam, p. 87–99.

753   Craig, M.J., Baas, J.H., Amos, K.J., Strachan, L.J., Manning, A.J., Paterson, D.M., Baker, M.L., 2020.

754   Biomediation of submarine sediment gravity flow dynamics. Geology, v. 48(1), p. 72–76.

755   https://doi.org/10.1130/G46837.1

756   Davis, C., Haughton, P., McCaffrey, W., Scott, E., Hogg, N., Kitching, D., 2009. Character and

757   distribution of hybrid sediment gravity flow deposits from the outer Forties Fan, Palaeocene

758   Central North Sea, UKCS. Marine and Petroleum Geology, v. 26, p. 1919–1939.

759   doi:10.1016/j.marpetgeo.2009.02.015.

760   Dominguez, R., 2007. Structural evolution of the Penguins Cluster, UK northern North Sea, *in* Jolley,

761   S.J., Barr, D., Walsh, J.J., Knipe, R.J., eds., Structurally Complex Reservoirs: Geological Society

762   Publishing House, Bath, pp. 25–48. doi:10.1144/sp292.2.

763   Dutkiewicz, A., Müller, R.D., O'Callaghan, S. and Jónasson, H., 2015. Census of seafloor sediments in

764   the world's ocean. Geology, 43, 795-798.

765   Felix, M. and Peakall, J., 2006. Transformation of debris flows into turbidity currents: mechanisms

766   inferred from laboratory experiments. Sedimentology, v. 53, p. 107-123.

767   Flint, S.S., Hodgson, D.M., Sprague, A.R., Brunt, R.L., van der Merwe, W.C., Figueiredo, J., Prelat, A.,

768   Box, D., Di Celma, C., Kavanagh, J.P., 2011. Depositional architecture and sequence stratigraphy

769   of the Karoo basin floor to shelf edge succession, Laingsburg depocentre, South Africa. Marine

770   and Petroleum Geology, v. 28, p. 658–674. doi:10.1016/j.marpetgeo.2010.06.008.

771   Fonnesu, M., Felletti, F., Haughton, P.D.W., Patacci, M., McCaffrey, W.D., 2018. Hybrid event bed

772   character and distribution linked to turbidite system sub-environments: The North Apennine

773   Gottero Sandstone (north-west Italy). Sedimentology, v. 65, p. 151-190,

774   doi:10.1111/sed.12376.

775 Fonnesu, M., Haughton, P., Felletti, F., McCaffrey, W., 2015. Short length-scale variability of hybrid

776   event beds and its applied significance. Marine and Petroleum Geology, v. 67, p. 583–603.

777   doi:10.1016/j.marpetgeo.2015.03.028

778 Franzese, J., Spalletti, L., Perez, I.G., Macdonald, D., 2003. Tectonic and paleoenvironmental

779   evolution of Mesozoic sedimentary basins along the Andean foothills of Argentina (32 degrees-

780   54 degrees S). Journal of South American Earth Sciences, v. 16, p. 81–90. doi:10.1016/s0895-

781   9811(03)00020-8.

782 Franzese, J.R., Spalletti, L.A., 2001. Late Triassic-early Jurassic continental extension in southwestern

783   Gondwana: tectonic segmentation and pre-break-up rifting. Journal of South American Earth

784   Sciences, v. 14, p. 257–270. doi:10.1016/s0895-9811(01)00029-3.

785 Gulisano, C.A., Gutiérrez Pleimling, A.R., 1995. The Jurassic of the Neuquén Basin. *in* Neuquén

786   Province: Buenos Aires, Asociación Geológica Argentina Field Guide, Serie E2, 111 p.

787 Guy, M., 1992. Facies analysis of the Kopervik sand interval, Kilda Field, Block 16/26, UK North Sea, *in*

788   Hardman, R.F.P., eds., Exploration Britian: Geological insights for the next Decade. Geological

789   Society of London Special Publication, v. 67, p. 187–220.

790 Haughton, P.D.W., Barker, S.P., McCaffrey, W.D., 2003. "Linked" debrites in sand-rich turbidite

791   systems - origin and significance. Sedimentology, v. 50(3), p. 459–482.

792 Haughton, P., Davis, C., McCaffrey, W., Barker, S., 2009. Hybrid sediment gravity flow deposits -

793   Classification, origin and significance. Marine and Petroleum Geology, v. 26, p. 1900–1918.

794   doi:10.1016/j.marpetgeo.2009.02.012.

795 Hofstra, M., Hodgson, D.M., Peakall, J., Flint, S.S., 2015. Giant scour-fills in ancient channel-lobe

796   transition zones: Formative processes and depositional architecture. Sedimentary Geology, v.

329, p. 98–114. doi:10.1016/j.sedgeo.2015.09.004.

Hofstra, M., Peakall, J., Hodgson, D.M., Stevenson, C.J., 2018. Architecture and morphodynamics of subcritical sediment waves in an ancient channel-lobe transition zone. Sedimentology, v. 65, p. 2339–2367. doi:10.1111/sed.12468.

Howell, J.A., Schwarz, E., Spalletti, L.A., Veiga, G.D., 2005. The Neuquen Basin: an overview. *in* Veiga, G.D., Spalletti, L.A., Howell, J.A., Schwarz, E., eds., Neuquen Basin, Argentina: A Case Study in Sequence Stratigraphy and Basin Dynamics. Geological Society Publishing House, Bath, p. 1–14. doi:10.1144/gsl.sp.2005.252.01.01.

Iverson, R.M., 1997. The physics of debris flows. Reviews of Geophysics, v. 35, p. 245–296.

Johnson, M.R., 1991. Sandstone petrography, provenance and plate tectonic setting in Gondwana context of the southeastern Cape-Karoo Basin. South African Journal of Geology, v. 94, p. 137–154.

Kane, I.A., McCaffrey, W.D., Martinsen, O.J., 2009. Allogenic vs. autogenic controls on megaflute formation. Journal of Sedimentary Research, v. 79, p. 643–651. doi:10.2110/jsr.2009.072.

Kane, I.A., Pontén, A.S.M., 2012. Submarine transitional flow deposits in the Paleogene Gulf of Mexico. Geology, v. 40, p. 1119–1122. doi:10.1130/g33410.1.

Kane, I.A., Pontén, A.S.M., Vangdal, B., Eggenhuisen, J.T., Hodgson, D.M., Spychala, Y.T., 2017. The stratigraphic record and processes of turbidity current transformation across deep-marine lobes. Sedimentology, v. 64, p. 1236–1273. doi:10.1111/sed.12346.

Leclair, S.F., Arnott, R.W.C., 2005. Parallel lamination formed by high-density turbidity currents. Journal of Sedimentary Research, v. 75, p. 1–5. doi:10.2110/jsr.2005.001.

Lee, S.H., Jung, W.Y., Bahk, J.J., Gardner, J.M., Kim, J.K., Lee, S.H., 2013. Depositional features of co-genetic turbidite-debrite beds and possible mechanisms for their formation in distal lobated

820   bodies beyond the base-of-slope, Ulleung Basin, East Sea (Japan Sea). Marine Geology, v. 346,

821   p. 124–140. doi:10.1016/j.margeo.2013.09.001.

822   Llambías, E.J., Leanza, H.A., Carbone, O., 2007. Evolución Tectono-magmática durante el pérmico al

823   Jurásico temprano en la Cordillera del Viento (37°05ꞌS - 37°15ꞌS): Nuevas evidencias

824   geológicas y geoquímicas Del Inicio de la Cuencas Neuquina. Revista de la Asociación Geológica

825   Argentina, v. 62, p. 217–235.

826   Lowe, D.R., 1982. Sediment gravity flows .2. Depositional models with special reference to the

827   deposits of high-density turbidity currents. Journal of Sedimentary Petrology, v. 52, p. 279–298.

828   Lowe, D.R., Guy, M., 2000. Slurry-flow deposits in the Britannia Formation (Lower Cretaceous), North

829   Sea: a new perspective on the turbidity current and debris flow problem. Sedimentology, v. 47,

830   p. 31–70. doi:10.1046/j.1365-3091.2000.00276.x

831   Lowe, D.R., Guy, M., Palfrey, A., 2003. Facies of slurry-flow deposits, Britannia Formation (Lower

832   Cretaceous), North Sea: implications for flow evolution and deposit geometry. Sedimentology,

833   v. 50, p. 45–80.

834   McCave, I.N., Manighetti, B., Robinson, S.G., 1995. Sortable silt and fine sediment size/composition

835   slicing: Parameters for palaeocurrent speed and palaeoceanography. Paleoceanography, v.

836   10(3), p. 593–610. https://doi.org/10.1029/94PA03039

837   McAnally, W.H., Friedrichs, C., Hamilton, D., Hayter, E., Shrestha, P., Rodriguez, H., Teeter, A., 2007.

838   Management of fluid mud in estuaries, bays, and lakes. I: Present state of understanding on

839   character and behavior. Journal of Hydraulic Engineering, v. 133(1), p. 9–22.

840   https://doi.org/10.1061/(ASCE)0733-9429(2007)133:1(9)

841   Malarkey, J., Baas, J.H., Hope, J.A., Aspden, R.J., Parsons, D.R., Peakall, J., Paterson, D.M., Schindler,

842   R.J., Ye, L., Lichtman, I.D., Bass, S.J., Davies, A.G., Manning, A.J., Thorne, P.D., 2015. The

843   pervasive role of biological cohesion in bedform development. Nature Communications, v. 6,

844   6257. doi:10.1038/ncomms7257.

845   Morris, P.H., Payne, S.N.J., Richards, D.P.J., 1999. Micropalaeontological biostratigraphy of the

846   Magnus Sandstone Member (Kimmeridgian-Early Volgian), Magnus Field, UK North Sea. *in*

847   Jones, R.W., Simmons, M.D., eds., Biostratigraphy in Production and Development Geology, v.

848   152, p. 55–73. doi:10.1144/gsl.sp.1999.152.01.04.

849   Mueller, P., Patacci, M., Di Giulio, A., 2017. Hybrid event beds in the proximal to distal extensive lobe

850   domain of the coarse-grained and sand-rich Bordighera turbidite system (NW Italy). Marine and

851   Petroleum Geology, v. 86, p. 908–931. doi:10.1016/J.MARPETGEO.2017.06.047.

852   Paim, P.S.G., Silveira, A.S., Lavina, E.L.C., Faccini, U.F., Leanza, H.A., Teixeira De Oliveira, J.M.M.,

853   D'Avila, R.S.F., 2008. High resolution stratigraphy and gravity flow deposits in the Los Molles

854   Formation (Cuyo Group - Jurassic) at La Jardinera region, Neuquén basin. Revista de la

855   Asociación Geológica Argentina, v. 63, p. 728–753.

856   Patacci, M., Haughton, P.D.W., McCaffrey, W.D., 2014. Rheological complexity in sediment gravity

857   flows forced to decelerate against a confining slope, Braux, SE France. Journal of Sedimentary

858   Research, v. 84, p. 270–277. doi:10.2110/jsr.2014.26.

859   Pierce, C.S., Haughton, P.D.W., Shannon, P.M., Pulham, A.J., Barker, S.P., Martinsen, O.J., 2018.

860   Variable character and diverse origin of hybrid event beds in a sandy submarine fan system,

861   Pennsylvanian Ross Sandstone Formation, western Ireland. Sedimentology, v. 65, p. 952–992.

862   doi:10.1111/sed.12412.

863   Piper, D.J.W., 1978. Turbidite muds and silts on deepsea fans and abyssal plains. In: Sedimentation in

864   Submarine Canyons, Fans and Trenches (Eds D.J.Stanley and G.Kelling), pp. 163–176. Dowden,

865   Hutchinsion and Ross, Stroudsburg, PA.

866   Prélat, A., Hodgson, D.M., Flint, S.S., 2009. Evolution, architecture and hierarchy of distributary

867   deep-water deposits: a high-resolution outcrop investigation from the Permian Karoo Basin,

868   South Africa. Sedimentology, v. 56, p. 2132-U25. doi:10.1111/j.1365-3091.2009.01073.x

869   Ravnås, R., Nøttvedt, A., Steel, R.J., Windelstad, J., 2000. Syn-rift sedimentary architectures in the

870   Northern North Sea, *in* Nøttvedt, A., eds., Dynamics of the Norwegein Margin, Geological

871   Society of London Special Publication, v. 167, p. 133–177. doi:10.1144/GSL.SP.2000.167.01.07.

872   Ravnås, R., Steel, R.J., 1997. Contrasting styles of Late Jurassic syn-rift turbidite sedimentation: A

873   comparative study of the Magnus and Oseberg areas, northern North Sea. Marine and

874   Petroleum Geology, v. 14, p. 417–449. doi:10.1016/s0264-8172(97)00010-x.

875   Schindler, R.J., Parsons, D.R., Ye, L., Hope, J.A., Baas, J.H., Peakall, J., Manning, A.J., Aspden, R.J.,

876   Malarkey, J., Simmons, S., Paterson, D.M., Lichtman, I.D., Davies, A.G., Thorne, P.D., Bass, S.J.,

877   2015. Sticky stuff: Redefining bedform prediction in modern and ancient environments.

878   Geology, v. 43, p. 399–402. doi:10.1130/g36262.1

879   Sixsmith, P.J., Flint, S.S., Wickens, H.D., Johnson, S.D., 2004. Anatomy and stratigraphic development

880   of a basin floor turbidite system in the Laingsburg Formation, main Karoo Basin, South Africa.

881   Journal of Sedimentary Research, v. 74, p. 239–254. doi:10.1306/082903740239.

882   Southard, J.B., 1991. Experimental determination of bedform stability. Annual Review of Earth and

883   Planetary Sciences, v. 19, p. 423–455. doi:10.1146/annurev.earth.19.1.423.

884   Southard, J.B., Boguchwal, L.A., 1990. Bed configurations in steady unidirectional water flows. 2.

885   Synthesis of flume data. Journal of Sedimentary Petrology, v. 60, p. 658–679.

886   Southern, S.J., Kane, I.A., Warchoł, M.J., Porten, K.W., McCaffrey, W.D., 2017. Hybrid event beds

887   dominated by transitional-flow facies: character, distribution and significance in the

888   Maastrichtian Springar Formation, north-west Vøring Basin, Norwegian Sea. Sedimentology, v.

889   64, p. 747–776. doi:10.1111/sed.12323.

890   Southern, S.J., Patacci, M., Felletti, F., McCaffrey, W.D., 2015. Influence of flow containment and

891   substrate entrainment upon sandy hybrid event beds containing a co-genetic mud-clast-rich

892   division. Sedimentary Geology, v. 321, p. 105–122. doi:10.1016/j.sedgeo.2015.03.006.

893   Spychala, Y.T., Hodgson, D.M., Flint, S.S., Mountney, N.P., 2015. Constraining the sedimentology and

894   stratigraphy of submarine intraslope lobe deposits using exhumed examples from the Karoo

895   Basin, South Africa. Sedimentary Geology, v. 322, p. 67–81. doi:10.1016/j.sedgeo.2015.03.013.

896   Spychala, Y.T., Hodgson, D.M., Prélat, A., Kane, I.A., Flint, S.S., Mountney, N.P., 2017. Frontal and

897   lateral submarine lobe fringes: Comparing sedimentary facies, architecture and flow processes.

898   Journal of Sedimentary Research, v. 87, p. 75–96. doi:10.2110/jsr.2017.2

899   Stevenson, C.J., Talling, P.J., Masson, D.G., Sumner, E.J., Frenz, M., Wynn, R.B., 2014. The spatial and

900   temporal distribution of grain-size breaks in turbidites. Sedimentology, v. 61, p. 1120–1156.

901   doi:10.1111/sed.12091.

902   Stow, D.A.V, Piper, D.J.W., 1984. Deep-water fine-grained sediments: facies models. In: Fine-Grained

903   Sediments: Deep-Water Processes and Facies. (Eds Stow, D.A.V. and Piper, D.J.W.) The

904   Geological Society, 15, p. 611–646.

905   Strachan, L.J., Bostock, H.C., Barnes, P.M., Neil, H.L., Gosling, M., 2016. Non-cohesive silt turbidity

906   current flow processes; insights from proximal sandy-silt and silty-sand turbidites, Fiordland,

907   New Zealand. Sedimentary Geology, v. 342, p. 118–132.

908   https://doi.org/10.1016/j.sedgeo.2016.06.017Sumner, E.J., Amy, L.A., Talling, P.J., 2008.

909   Deposit structure and processes of sand deposition from decelerating sediment suspensions.

910   Journal of Sedimentary Research, v. 78, p. 529–547. doi:10.2110/jsr.2008.062.

911   Sumner, E.J., Talling, P.J., Amy, L.A., 2009. Deposits of flows transitional between turbidity current

912   and debris flow. Geology, v. 37, p. 991–994. doi:10.1130/g30059a.1

913   Sylvester, Z., Lowe, D.R., 2004. Textural trends in turbidites and slurry beds from the Oligocene flysch

914   of the East Carpathians, Romania. Sedimentology, v. 51, p. 945–972. doi:10.1111/j.1365-

915   3091.2004.00653.x

916   Talling, P.J., 2013. Hybrid submarine flows comprising turbidity current and cohesive debris flow:

917   Deposits, theoretical and experimental analyses, and generalized models. Geosphere, v. 9, p.

918   460–488. doi:10.1130/ges00793.1

919   Talling, P.J., Amy, L.A., Wynn, R.B., Peakall, J., Robinson, M., 2004. Beds comprising debrite

920   sandwiched within co-genetic turbidite: origin and widespread occurrence in distal depositional

921   environments. Sedimentology, v. 51, p. 163–194. doi:10.1046/j.1365-3091.2003.00617.x

922   Talling, P.J., Masson, D.G., Sumner, E.J., Malgesini, G., 2012. Subaqueous sediment density flows:

923   Depositional processes and deposit types. Sedimentology, v. 59, p. 1937–2003.

924   doi:10.1111/j.1365-3091.2012.01353.x

925   Talling, P.J., Wynn, R.B., Masson, D.G., Frenz, M., Cronin, B.T., Schiebel, R., Akhmetzhanov, A.M.,

926   Dallmeier-Tiessen, S., Benetti, S., Weaver, P.P.E., Georgiopoulou, A., Zuhlsdorff, C., Amy, L.A.,

927   2007. Onset of submarine debris flow deposition far from original giant landslide. Nature, v.

928   450, p. 541–544. doi:10.1038/nature06313.

929   Tankard, A., Welsink, H., Aukes, P., Newton, R., Stettler, E., 2009. Tectonic evolution of the Cape and

930   Karoo basins of South Africa. Marine and Petroleum Geology, v. 26, p. 1379–1412.

931   doi:http://dx.doi.org/10.1016/j.marpetgeo.2009.01.022

932   Van den Berg, H.H., van Gelder, A., 1993. A new bedform stability diagram with emphasis on the

933   transition of ripples to plane bed in flows over fine sand and silt. *in* Marzo, M. and

934   Puigdefabregas, C., eds., Alluvial Sedimentation: International Association of Sedimentologists

935   Special Publications, v. 17, p. 11–21.

936 Vergani, G.D., Tankard, A.J., Belotti, H.J., Welsink, H.J., 1995. Tectonic evolution and paleogeography

937   of the Neuquén Basin, Argentina. *in* Tankard, A.J., Suarez, S. Welsink, H.J., eds., Petroleum

938   Basins of South America: American Association of Petroleum Geologists Memoir, v. 62, p. 383–

939   402.

940 Visser, J.N.J., 1993. Sea-level changes in a back-arc-foreland transition: the late Carboniferous-

941   Permian Karoo Basin of South Africa. Sedimentary Geology, v. 83, p. 115–131.

942   doi:http://dx.doi.org/10.1016/0037-0738(93)90185-8.

943 Vrolijik, P.J., Southard, J.B., 1997. Experiments on rapid deposition of sand from high-velocity flows.

944   Geoscience Canada, v. 24, p. 45–54.

945 Weaver, C.E., 1989. Clays, muds and shales. Elsevier, Developments in Sedimentology, 44,

946   Amsterdam.

947 Wickens, H. de V, 1994. Basin floor fan building turbidites of the southwestern Karoo Basin, Permain

948   Ecca Group, South Africa [PhD Thesis]. University of Port Elizabeth.

949 Winterwerp, J.C., W.G.M. van Kesteren, 2004. Introduction to the Physics of Cohesive Sediments in

950   the Marine Environment, Developments in Sedimentology, 56, Elsevier, New York, 466 pp.

951 Wood, A., Smith, A.J., 1958. The sedimentation and sedimentary history of the Aberystwyth Grits

952   (Upper Llandoverian). Quarterly Journal of the Geological Society, v. 114, p. 163–195.

953

954 Figure captions

955

956 **Figure 1.** Cartoon logs with example core photos illustrating banded sandstone facies and hybrid

957 beds documented from the Britannia and Springar formations (1-4) and the Paleogene Forties Fan,

958 North Sea (5-6). Britannia and Springar banding (top left) occurs in exceptionally thick divisions

959 several meters thick with individual bands several centimeters thick (up to >50 cm thick) associated

960 with abundant dewatering pipes. Core photos, upper center, show thick macrobanding (dark brown)

961 transitioning upwards into thinner mesobanding (light brown). Megabanding is shown on the right

962 hand side. Arrows highlight individual dirty bands (modified from Lowe and Guy, 2000; their Fig. 10).

963 Banding in the Forties Fan is included within the idealized hybrid bed model of Haughton et al.

964 (2009), whereby it occurs as a decimeter thick division sandwiched between a clean basal sandstone

965 and an overlying linked-debrite (bottom left). Individual bands are typically several centimeters

966 thick. The lowermost core photo shows banding within a hybrid bed within the Everest field, well

967 section depth 8569-8564 ft (modified after Haughton et al., 2009; their Fig. 6). Note that banded

968 divisions can be sand-prone or argillaceous in character. The key refers also to Figures 3, 5, 6, 7, 8, 11

969 and 14. Banding is represented as mudstone stripes (grey), however this covers dirty bands with a

970 variety of different sandstone contents. References: 1) Lowe and Guy (2000), 2) Lowe et al. (2003),

971 3) Barker et al. (2008), 4) Southern et al. (2017), 5) Haughton et al. (2009), and 6) Davis et al. (2009).

972

973 **Figure 2.** Geological setting of the Magnus oilfield. (A) The Magnus oilfield is situated in the NW

974 margin of the Viking Graben between the Møre Basin, and the Magnus-Penguin Basin to the SE. (B)

975 Core locations and major structures across the Magnus oilfield (note M16 is core used in this study).

976 Magnus Sandstone Member (MSM) depocenters are marked for MSM-A (fault controlled channel

977 sandstones through the central part of the field); MSM-B (field-wide MTD that also covers MSM-A),

978 and; MSM-C and E (with a lobe-like depocenter to the SE) adapted from Morris et al. (1999). (C)

979 Stratigraphy of the Magnus oilfield comprises a sandstone-rich turbidite interval called the Magnus

980 Sandstone Member (MSM), which is bounded above and below by the mud-rich intervals of the

981 Upper and Lower Kimmeridge Clay formations, respectively. The interval examined in this paper is

982 within the lower part of the MSM succession.

983

984 **Figure 3.** Sedimentary log from the upper part of MSM-B (mud-rich mass transport deposit), through

985 MSM-C (muddy turbidites) and into MSM-E (clean turbidites). The spatial distribution of these

986 intervals across the field is shown in Figure 2B. Note the MSM-C turbidites are dirty compared to the

987 overlying MSM-E turbidite stratigraphy with almost all beds recording some form of mud-rich

988 banding (see Fig. 1 for key). Banding occurs in a variety of positions in the beds. Details of selected

989 beds are shown in Figure 4.

990

991 **Figure 4.** Details of banded facies within the Magnus MSM-C turbidites. Dirty bands are composed of

992 a large amount of rounded sub-millimeter diameter mudstone clasts and an elevated proportion of

993 matrix. (A) Thin sub-parallel mud-rich dirty bands containing isolated floating sand grains, which are

994 intercalated with cleaner bands composed of planar-laminated sandstone. (B) Thicker bands with

995 sharp mud-rich bases grading upwards into cleaner bands, which founder down into the muddier

996 underlying band. (C) Thin sub-parallel, low-angle and wavy mud-rich bands with isolated floating

997 sand grains. Dirty bands have loaded upper contacts with the overlying cleaner bands. BGS sample

998 numbers for thin sections: (A) SSK54784 (B) SSK54786 (C) SSK54787.

999

1000 **Figure 5.** Geological setting of the Neuquén Basin. (A) Showing the extent of the Neuquén Basin,

1001 bounded on each side by orogenies. Outcrops used to examine banded sandstones are situated near

1002 the towns of Chos Malal (1) and Aluminé (2), marked with red stars on the GoogleEarth[TM] inserts. (B)

1003 Stratigraphic context of the sections presented in this study, which sit within the Early/Middle

1004 Jurassic Los Molles Formation. (C) Stratigraphy through the Los Molles Formation, showing deep-

1005   marine mudstones (black) punctuated by sandy turbidite deposition (yellow), coarse gravels and

1006   conglomerate deposits (orange), and mass transport deposits (green) (after Gulisano and Gutiérrez

1007   Pleimling, 1995; Llambías et al., 2007). See Fig. 1 for key. Studied sections (red stars) are described in

1008   more detail in Figs 6, 7 and 8.

1009

1010   **Figure 6.** Chos Malal Roadside Gully (see Fig. 5 for stratigraphic position). (A) Outcrop showing an

1011   erosion surface (red dashed line) (marked 1) cutting into a chaotic mud-rich sandstone, which is

1012   overlain by mud clast conglomerate (between 1 and 2) that grades laterally into thinner mudstone

1013   clast horizons. In turn, this is overlain by amalgamated banded sandstone beds (between 2 and 3).

1014   The banded sandstone is overlain by a clast supported gravel bed (marked 3) containing intra- and

1015   extra-formational mudstone and sandstone clasts (see Fig. 1 for key). (B) Close up of bands in Part A,

1016   showing they are discontinuous and composed of small elongated mud clasts. (C) Shows outcrop 100

1017   m across strike from Part A with the erosion surface (1), overlain by amalgamated banded

1018   sandstones (inferred bed contact shown as red dashed line), and the gravel bed (3). Banded divisions

1019   are variable in thickness laterally, occur towards the tops of beds and become more mud-rich

1020   upwards. Note that the lowermost banded sandstones are laterally equivalent to the mud-clast

1021   conglomerate in Part A. (D) Individual bands vary in thickness laterally, are sub-parallel to very low-

1022   angle and composed of a large amount of mudstone clasts. (E) Thin section of a zone of banded

1023   sandstone with a relatively low proportion of total mudstone (plane polarised light left, and cross-

1024   polarised light right). Note the weakly developed cleaner bands with occasional mudstone clasts

1025   (white dashed lines). Lens cap in A, C and D is 7 cm diameter. White arrows highlight banded

1026   sandstone divisions or individual dirty bands (Parts C and D respectively).

1027

1028 **Figure 7.** Chos Malal Roadside Cutting (see Fig. 5 for stratigraphic position). Turbidite sandstones

1029 with distinct styles of banding. (A) Sedimentary log of Part B, showing amalgamated banded beds

1030 with erosional bases and mud clast conglomerate lags (see Fig. 1 for key). (B) Beds have lateral and

1031 vertical heterogeneity in facies with lenticular mud clast conglomerate lags and variable styles of

1032 banding. (C) Progression of banding styles upwards within an individual bed. At the base is a sand-

1033 prone division with sub-parallel bands (B_{PS}) that pinch and swell over decimeters and are commonly

1034 discontinuous. This is sharply overlain by (B_{PM}) a mud-prone division with slightly thicker (up to 1 cm)

1035 sub-parallel dirty bands and separated by thinner cleaner bands. In turn, this is sharply overlain by

1036 (B_{CL}) that is composed of complex low-angle heterolithic banding with bands forming lenses over 10-

1037 15 cm. This low-angle banding grades upwards into more steeply dipping ripple-like mud-rich

1038 bedforms (B_{CR}). Lens cap is 7 cm diameter.

1039

1040 **Figure 8.** La Jardinera Road Cutting Outcrop. (A) Outcrop showing the across strike architecture of a

1041 succession of thin to medium-bedded sandstones. Flow direction into page. (B) Sedimentary log of

1042 outcrop in Part A (see Fig. 1 for key) with supporting photographs showing: (C) a linked-debrite with

1043 mudstone and banded sandstone clasts, (D) a sub-parallel banded sandstone division at the top of a

1044 bed with significant lateral variation in the amount of mudstone clasts, (E) a sub-parallel banded

1045 division overlying a structureless sandstone, and (F) relatively thin bedded sub-parallel banded

1046 sandstones. Bed bases (red dashed lines) and internal bed facies divisions (white dashed lines) are

1047 marked. White arrows highlight banded divisions. Lens cap is 7 cm diameter.

1048

1049 **Figure 9.** Thin sections taken from La Jardinera road cutting outcrop (see Figs 8D and 8F for location

1050 of samples). (A) Thin section from a banded interval overlying a thin bedded sandstone, showing

1051 dirty bands composed of a large amount of small-diameter mudstone clasts and an elevated

1052   proportion of matrix mudstone compared to the cleaner bands. Cleaner bands are loaded into the

1053   upper contacts of the mud-rich bands. Note that the bands are sub-parallel to low angle with

1054   thickness variations seen over centimeters. (B) Laterally equivalent section over meters to Part A,

1055   showing scattered mud clasts within a poorly sorted cleaner sandstone with an increasing

1056   abundance of mudstone clasts upwards into a dirty band. (C) Thin section across the boundary

1057   between a dirty band, composed primarily of rounded mudstone clasts that decrease in abundance

1058   upwards, and an overlying cleaner band with much better sorting and occasional sub-millimeter

1059   mudstone clasts.

1060

1061   **Figure 10.** Geological setting of the Laingsburg depocenter, Karoo Basin, South Africa. Top left

1062   showing stratigraphy and interpretation of paleoenvironments (after Flint et al., 2011), and bottom

1063   right the paleo-reconstruction of the fan environment (based on Sixsmith et al., 2004; Hofstra et al.,

1064   2015). The Geelbek outcrop is situated in a relatively proximal basin-floor to base-of-slope setting

1065   within the axis of deposition of Unit A5, and close to channels.

1066

1067   **Figure 11.** (A) Sand-prone succession of thin to medium bedded sandstones within Unit 4 of the

1068   Lainsburg depocenter, Geelbek River, Karoo Basin (see Fig. 1 for key). Banding typically occurs

1069   towards bed tops and presents a variety of morphologies. (B) Sub-parallel dirty bands intercalated

1070   with cleaner bands showing faint planar lamination. (C) A complex heterolithic bedform comprising

1071   steeply dipping muddy foresets on the left, which transition downstream into low-amplitude

1072   sandstone and mudstone bedwaves. White arrows highlight dirty bands. Lens cap 7 cm diameter.

1073

1074   **Figure 12.** Proportion of total mud content (matrix and mudstone clasts) versus detrital grain

1075   content within individual bands. Nq are samples from the Neuquén Basin and Mg are samples from

1076   the Magnus oilfield. The yellow circle shows mudstone contents in a dirty band described from the

1077   Carpathian Flysch (Sylvester and Lowe, 2004). Note the range of mud content in both dirty and

1078   cleaner bands from mud-rich to sand-rich dirty bands, and the continuum into mud-rich and sand-
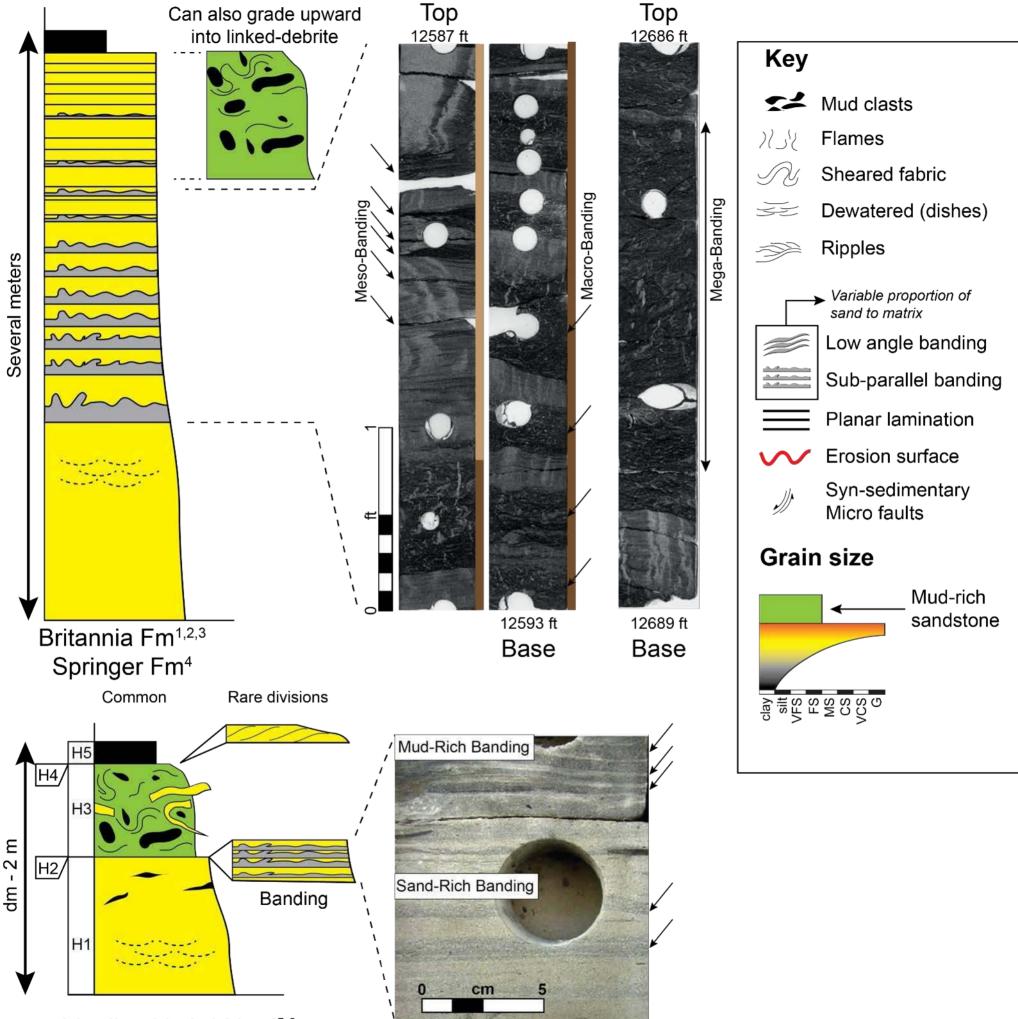
1079   rich cleaner bands.

1080

1081   **Figure 13.** Comparison of banded sandstone from the field (this study; Figs 4B and 11C) with mixed

1082   mud/sand stratification from the experiments of Baas et al. (2016). Note the similarities between

1083   heterolithic banding in the field and mixed sand/mud stratification in the experiments. Variations in

1084   banding morphology are likely linked with flow velocity and the balance of turbulent versus cohesive

1085   forces near to the bed (see main text for more detail). Flow regimes shown are Washed Out Ripples

1086   (WOR) and Upper Stage Plane Bed (USPB).
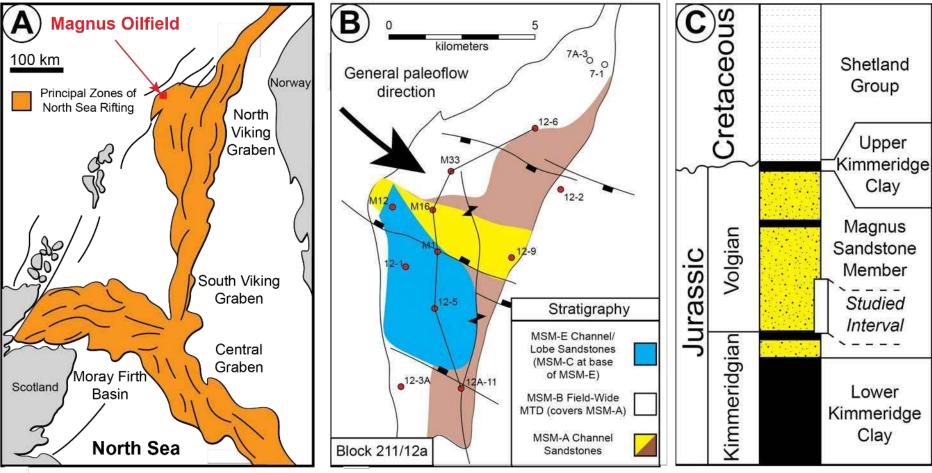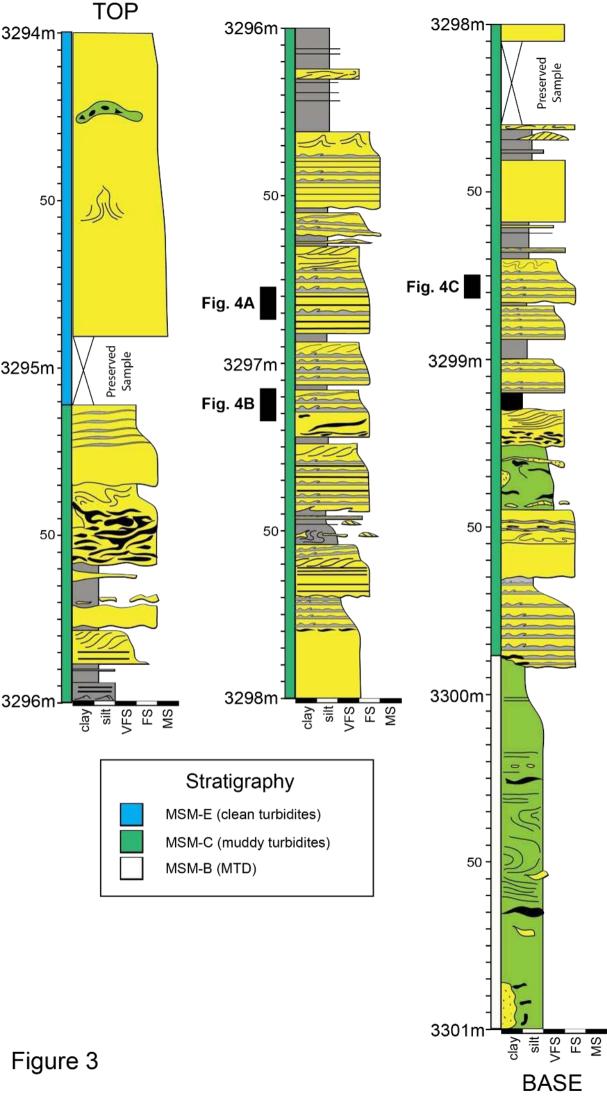
1087

1088   **Figure 14.** Conceptual phase space showing how deposit character changes with the cohesive

1089   strength of the flow (mud content) and rate of flow deceleration (linked to rate of aggradation). In

1090   addition, with increasing cohesive strength flows will decelerate more rapidly, ultimately depositing

1091   en masse. Example deposits are sourced from experiments on mixed sand/mud suspensions: 1)

1092   Sumner et al. (2009), 2) Baas et al. (2011), 3) Baas et al. (2016) and, 4) field deposits from this study.

1093 D_b = mud-rich debrite. L-D_b = linked-debrite. ST = clean structureless sandstone. B_P = sub-parallel

1094   banding (e.g. Fig. 4B). B_{CL} = low-angle complex heterolithic banding (e.g. Fig. 11C). B_{CR} = higher-angle

1095   complex banding at ripple-scale (e.g. Fig. 7C). PL = planar lamination. RXL = rippled cross-laminated

1096   sand. Note that linked-debrites and banded sands are produced from flows with relatively high

1097   cohesive strength (i.e. high mud content). However, banded sandstones require slower deceleration

1098   rates (a prolonged period of traction) to form than linked debrites.

1099

1100   **Figure 15.** (A) Conceptual model of the distribution of clean turbidite sandstone, banded sandstone

1101   and linked-debrites across a deep-water clastic system. Banded sandstones are postulated to be

1102   relatively proximal facies found close to sites of erosion into muddy substrates: (i) early intraslope

1103   lobes, (ii) immediately down dip of channel mouth scours and proximal lobe settings, and (iii)

1104   channel splays. (iv) Linked-debrites are a relatively distal facies associated with distal and lateral lobe

1105   fringes. (v) Flows interacting with basin topography can produce banded sandstones and linked-

1106   debrites local to the base of confining slopes. (B) Interpreted steadiness of flows at proximal and

1107   distal locations (adapted from Kane et al., 2009; Stevenson et al., 2014). Proximally, rate of flow

1108   deceleration is slow with a period of traction at the bed, which promotes deposition of banded

1109   sandstones. Distally, flow deceleration is rapid and deposits are emplaced en-masse with minimal

1110   traction, resulting in deposition of linked-debrites. (C) Conceptual facies tract produced by

1111   transitional flows showing the evolution of deposits from the site of mud entrainment (adapted

1112   from Kane et al., 2017; Fonnesu et al., 2017). Flows entrain mud and become mixed

1113   cohesive/turbulent suspensions. The balance of cohesive versus turbulent forces and rate of flow

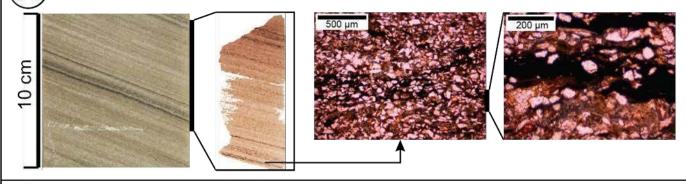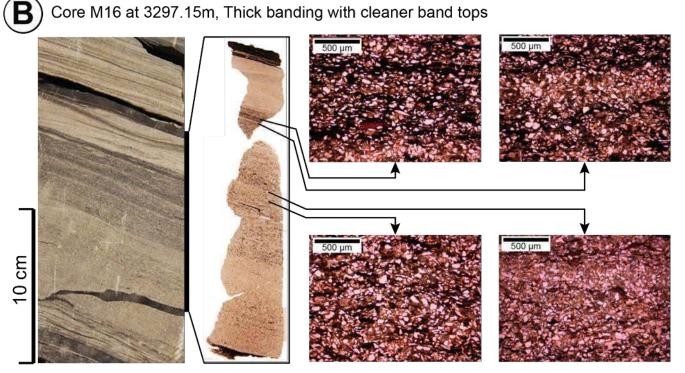1114   deceleration governs the style of deposition (see main text for details).

1115

Can also grade upward into linked-debrite

Several meters

Britannia Fm[1,2,3]
Springer Fm[4]

Top 12587 ft

Meso-Banding

Macro-Banding

Mega-Banding

Top 12686 ft

ft

12593 ft
Base

12689 ft
Base

Key

- Mud clasts
- Flames
- Sheared fabric
- Dewatered (dishes)
- Ripples

Variable proportion of sand to matrix

- Low angle banding
- Sub-parallel banding
- Planar lamination
- Erosion surface
- Syn-sedimentary Micro faults

Grain size

Mud-rich sandstone

clay silt VFS FS MS CS VCS G

Common

Rare divisions

H5
H4
H3
H2
H1

dm - 2 m

Banding

Idealized hybrid bed[5,6]

Mud-Rich Banding

Sand-Rich Banding

0   cm   5

Figure 2

TOP

3294m

50

3295m

Preserved Sample

50

3296m

clay | silt | VFS | FS | MS

3296m

50

3297m

Fig. 4A

Fig. 4B

50

3298m

clay | silt | VFS | FS | MS

3298m

Fig. 4C

50

3299m

50

3300m

50

3301m

clay | silt | VFS | FS | MS

Preserved Sample

BASE

Stratigraphy

MSM-E (clean turbidites)
MSM-C (muddy turbidites)
MSM-B (MTD)

Figure 3

A Core M16 at 3296.85m, Thin banding with PL

B Core M16 at 3297.15m, Thick banding with cleaner band tops

C Core M16 at 3298.82m, Discontinuous banding

Figure 4

Figure 5

Flow direction into page

Part C

Part B

3

2

1

1m

2m

1m

0

clay · silt · VFS · FS · MS · CS · VCS · G

3

2

1

B

Sample MMA

E

1 mm

1 mm

15

10

5

0

mm

C

3

Part D

Part A

1

D

A

9m

8m

clay | silt | VFS | FS | MS | CS | VCS

B

Part C

1m

C

M

B_{CR}

B_{CL}

B_{PM}

B_{PS}

Canon

Figure 8

A

Cleaner sandstone bands

Loaded upper contacts

Low angle downlap and lateral amalgamation of bands

1cm

1000 µm

500 µm

B

Sub-millimeter mudstone clasts

Larger rounded mudstone clast

Increasing mudstone clast abundance

1cm

1000 µm

8 mm

C

Base of overlying dirty band

Cleaner band

Mudstone clast-rich base to dirty band

Decreasing mudstone clast abundance

Cleaner band

Dirty band

1cm

1000 µm

4 mm

Figure10

Field Deposits	Experimental Deposits

Figure 11C

5 cm

Figure 4B

5 cm

Bed scour — Mud foresets — Sandy mud bedwave

WOR

Muddy sand low-angle foresets

USPB

5 cm

USPB

Composite scour and low-angle bedforms

Sub-parallel banding

Cleaner sand   Sandy mud

Muddy sand   Mud

Figure 14

Figure 15